Electronic Supplementary Information

A facile synthesis methodology for preparation of Ag- Ni - Reduced Graphene Oxide: A magnetically separable versatile nanocatalyst for multiple organic reactions and Density Functional Study of its electronic structures

*Madhurya Chandel, Priyanka Makkar, Barun Kumar Ghosh, Debabrata Moitra, Narendra Nath Ghosh**

Nano-Materials Lab, Department of Chemistry, Birla Institute of Technology and Science, Pilani K. K. Birla Goa Campus, Zuarinagar, Goa 403726, India.

Synthesis of the materials

Synthesis of graphene oxide (GO)

Graphene oxide was synthesized by using the modified Hummers method.[1] In this method, 1 g of graphite powder and 0.6 g of $NaNO_3$ were mixed with 35 ml of H_2SO_4 at 0 °C. The mixture was stirred for 6 h, and then 3.8 g of $KMnO_4$ was added. The temperature was maintained at 35 °C for 8 h for complete oxidation process. After that, 60 ml of deionized water was added slowly and maintained the temperature at 98 °C for 1 h. Then 2 ml of 30% H_2O_2 was added and stirred for 0.5 h. The mixture was centrifuged, and then washed with 10% HCl, followed by distilled water. The yellowish brown precipitate of graphene oxide was obtained and dried at 60 °C.

Synthesis Methodology of $(Ag_{0.27}Ni_{0.73})_{37}RGO_{63}$

The synthesis of $(Ag_{0.27}Ni_{0.73})_{37}RGO_{63}$ which is composed of 10 wt % Ag, 27 wt% Ni, and 63 wt% RGO, was conducted in two steps. In the first step, graphene oxide (GO) was prepared by using the modified Hummers method.[1] In the next step, a mixture of (21.13 ml) ethylene glycol and (0.469 mg) PVP (molar ratio 2:1) was prepared and 157.5 mg of GO was dispersed in this mixture. In this dispersion, 39.36 mg of $AgNO_3$ and 334.46 mg of $Ni(NO_3).6H_2O$ were added. After addition of metal nitrate salts, the mixture was stirred till salts were dissolved. In this mixture, NaOH (0.469 mg) pellets was added with stirring till the pH of the mixture became ~10, and then N_2H_4 (2.81 ml) was added dropwise keeping metal ion: N_2H_4 molar ratio of 1:40. After complete addition of N_2H_4, the reaction mixture was refluxed at 85 ^oC for 15 min. Then it was cooled to room temperature and precipitate thus formed was magnetically separated from the reaction mixture by using magnet externally. The collected precipitate was washed with distilled water until the pH of the washing reaches ~7. Finally, the precipitate was washed with acetone,

and then dried at 60 °C for 10 h. The formation and purity of the $(Ag_{0.27}Ni_{0.73})_{37}RGO_{63}$ was confirmed using XRD.

Table S1. Codes of the catalyst and the corresponding compositions $(Ag_xNi_{(1-x)})_yRGO_{(100-y)}$.

Entry	Catalyst code	Weight% of the composites		
		Ag	Ni	RGO
1	Pure Ni	0	100	0
2	Pure Ag	100	0	0
3	$Ni_{10}RGO_{90}$	0	10	90
4	$Ni_{20}RGO_{80}$	0	20	80
5	$Ni_{30}RGO_{70}$	0	30	70
6	$Ni_{40}RGO_{60}$	0	40	60
7	$Ag_{0.5}Ni_{0.95}$	5	95	0
8	$Ag_{0.15}Ni_{0.85}$	15	85	0
9	$Ag_{0.25}Ni_{0.75}$	25	75	0
10	$Ag_{0.27}Ni_{0.73}$	27	73	0
11	$Ag_{0.50}Ni_{0.50}$	50	50	0
12	$(Ag_{0.05}Ni_{0.95})_{90}RGO_{10}$	4.5	85.5	10
13	$(Ag_{0.05}Ni_{0.95})_{70}RGO_{30}$	3.5	66.5	30
14	$(Ag_{0.05}Ni_{0.95})_{60}RGO_{40}$	3	57	40
15	$(Ag_{0.05}Ni_{0.95})_{50}RGO_{50}$	2.5	47.5	50
16	$(Ag_{0.05}Ni_{0.95})_{40}RGO_{60}$	2	38	60
17	$(Ag_{0.15}Ni_{0.85})_{33.5}RGO_{66.5}$	5	28.5	66.5
18	$(Ag_{0.27}Ni_{0.73})_{37}RGO_{63}$	10	27	63
19	$(Ag_{0.37}Ni_{0.63})_{40.5}RGO_{59.5}$	15	25.5	59.5

20	$(Ag_{0.45}Ni_{0.55})_{44}RGO_{56}$	20	24	56

Characterization and Instrumentation

Room temperature powder X-ray diffraction (XRD) patterns of the synthesized materials were recorded using a powder X-ray diffractometer (Mini Flex II, Rigaku, Japan) with Cu K_α (λ = 0.15405 nm) radiation at a scanning speed of 3° min^{-1}. Fourier Transform Infrared spectra (FT-IR) were recorded in KBr by using spectrophotometer (IR Affinity-1, Shimadzu, Japan). Thermogravimetric analysis (TGA) was carried out using DTA-60 (Shimadzu, Japan). Field Emission Scanning Electron Microscope (FESEM) images of samples were obtained using Quanta 250 FEG (FEI). Energy dispersive X-ray spectra of the synthesized materials were recorded using an EDAX ELEMENT electron microscope. Raman spectra were recorded on a Renishawin Via Raman microscope with a 633 nm laser excitation. Room temperature magnetization with respect to an external magnetic field was measured for the synthesized catalysts using a Vibrating Sample Magnetometer (VSM) (EV5, ADE Technology, USA). Liquid Chromatography-Mass Spectrometer (LC-MS) full scan spectra were recorded on Agilent LC-MS for the product obtained from A3 coupling and 'Click reaction'. ^1H NMR (Nuclear Magnetic Resonance) spectra were recorded on a BRUKER 400 ULTRA SHIELD PLUS (400 MHz) instrument using deuterated solvent. The gas chromatograph was carried out using (Shimadzu GC-2014) equipped with a capillary column (30 M × 0.25 mm × 0.25 mm) and a FID detector. Differential Scanning Calorimetric (DSC) analysis was carried out using DSC-60 (Shimadzu, Japan) to determine the melting point of the products obtained from Click reaction.

Computational details

In case of Ag and Ni unit cell (space group Fm-3m (225)) a Monkhorst-Pack mesh[2] of k-points 8×8×8 is used, to sample the Brillouin zone for geometry optimization and for calculating the density of states.

Ag and Ni slab was constructed using Ag and Ni unit cell. The crystal was cleaved along (111) plane with four layer slab and vacuum space 10 Å along z direction. Here, 4×4×1 *k* point grids were used for optimization of structure and density of states calculations, respectively.

The initial superlattice structure of graphene was constructed using a 2×2×1 super cell with 8 atoms and 15 Å vacuum space at z-axis and optimized using 4×4×1 Monkhorst-Pack *k* point grid.[2, 3]

The Ag-Ni interface was constructed with Ni (111) slab placed 3 Å above the Ag (111) slab and 15 Å vacuum space at z-axis. Here, 4×4×1 *k* point grids were used for optimization of structure and density of states calculations, respectively. The Ag-Ni-graphene superlattice was constructed with Ag-Ni interface placed 3 Å above the monolayer graphene and 15 Å vacuum space at z-axis. Here, 4×4×1 *k* point grids were used for optimization of structure and density of states calculations respectively. The sizes of the unit cells of the systems simulated are listed in Table S1.

Table S2. The sizes of the unit cells of simulated systems.

System	Structural parameters	
Ag unit cell	a= b = c = 4.08 Å	$\alpha = \beta = \gamma = 90^o$
Ni unit cell	a= b = c = 3.52 Å	$\alpha = \beta = \gamma = 90^o$
Graphene	a= b = 4.9 Å ; c = 31.1 Å	$\alpha = \beta = 90^o$, $\gamma = 120^o$
Ag-slab	a= b = 2.89 Å ; c = 18.8 Å	$\alpha = \beta = 90^o$, $\gamma = 120^o$

Ni-slab	a= b = 2.49 Å ; c = 21.1 Å	$\alpha = \beta = 90^o$, $\gamma = 120^o$
Ag-Ni	a= b =4.99 Å; c = 29.5 Å	$\alpha = \beta = 90^o$, $\gamma = 120^o$
Ag-Ni-graphene	a= b = 8.26Å; c = 25.3 Å	$\alpha = \beta = 90^o$, $\gamma = 120^o$
Strain on interface	ε_{11}= 1.46 % , ε_{12}= 1.49 %	
	Mean Absolute Strain = 3.66 %	

Details of the input files for geometric optimization of the Ni unit cell, Ag unit cell, graphene superlattice, Ni (111) slab, Ag (111) slab, Ag-Ni Interface, and Ag-Ni-graphene superlattice

Ni-unit cell

```
 &CONTROL
                title = 'Ni' ,
           calculation = 'vc-relax' ,
          restart_mode = 'from_scratch' ,
               outdir = '/home/madhuriya/Ag-Ni/vdW/Ni-unit-cell/' ,
               wfcdir = '/home/madhuriya/Ag-Ni/vdW/Ni-unit-cell/' ,
            pseudo_dir = '/opt/apps/quantum_espresso/qe-
6.1/pseudo/pslibrary.1.0.0/pbe/PSEUDOPOTENTIALS/' ,
               prefix = 'pwscf' ,
            verbosity = 'low' ,
/
 &SYSTEM
                ibrav = 2,
            celldm(1) = 6.6610956165d0,
                  nat = 1,
                 ntyp = 1,
              ecutwfc = 30.0 ,
              ecutrho = 240.0 ,
            input_dft = 'pbe' ,
          occupations = 'smearing' ,
              degauss = 0.02 ,
             smearing = 'methfessel-paxton' ,
                nspin = 2 ,
  starting_magnetization(1) = 0.1,
             vdw_corr = 'grimme-d2' ,
/
 &ELECTRONS
        electron_maxstep = 500,
       scf_must_converge = .true. ,
             conv_thr = 1.0e-8 ,
```

```
            mixing_beta = 0.7 ,
/
&IONS
            ion_dynamics = 'bfgs' ,
/
&CELL
/
ATOMIC_SPECIES
  Ni   58.69000  Ni.pbe-n-rrkjus_psl.1.0.0.UPF
ATOMIC_POSITIONS crystal
  Ni      0.000000000    0.000000000    0.000000000
K_POINTS automatic
 8 8 8   0 0 0
```

Ag-unit cell

```
&CONTROL
                title = 'Ag' ,
            calculation = 'relax' ,
            restart_mode = 'from_scratch' ,
                outdir = '/home/madhuriya/Ag-Ni/vdW/Ag-unit-cell/' ,
                wfcdir = '/home/madhuriya/Ag-Ni/vdW/Ag-unit-cell/' ,
            pseudo_dir = '/opt/apps/quantum_espresso/qe-
6.1/pseudo/pslibrary.1.0.0/pbe/PSEUDOPOTENTIALS/' ,
                prefix = 'pwscf' ,
            verbosity = 'low' ,
/
&SYSTEM
                ibrav = 2,
            celldm(1) = 7.7217988902d0,
                nat = 1,
                ntyp = 1,
            ecutwfc = 25 ,
            ecutrho = 225 ,
            input_dft = 'pbe' ,
            occupations = 'smearing' ,
            degauss = 0.005d0 ,
            smearing = 'methfessel-paxton' ,
            vdw_corr = 'grimme-d2' ,
/
&ELECTRONS
        electron_maxstep = 500,
            conv_thr = 1d-07 ,
            mixing_mode = 'local-TF' ,
            mixing_beta = 0.7d0 ,
/
&IONS
            ion_dynamics = 'bfgs' ,
/
ATOMIC_SPECIES
  Ag  107.86800  Ag.pbe-n-rrkjus_psl.1.0.0.UPF
```

```
ATOMIC_POSITIONS crystal
   Ag      0.000000000    0.000000000    0.000000000
K_POINTS automatic
  8 8 8   0 0 0
```

Ag (111)-slab

```
&CONTROL
                title = 'Ag' ,
            calculation = 'relax' ,
           restart_mode = 'from_scratch' ,
                outdir = '/home/madhuriya/Ag-Ni/vdW/Ag-Slab/' ,
                wfcdir = '/home/madhuriya/Ag-Ni/vdW/Ag-Slab/' ,
            pseudo_dir = '/opt/apps/quantum_espresso/qe-
6.1/pseudo/pslibrary.1.0.0/pbe/PSEUDOPOTENTIALS/' ,
                prefix = 'pwscf' ,
             verbosity = 'high' ,
 /
 &SYSTEM
                ibrav = 0,
            celldm(1) = 5.4601363582d0,
                  nat = 4,
                 ntyp = 1,
              ecutwfc = 25 ,
              ecutrho = 250 ,
            input_dft = 'pbe' ,
           occupations = 'smearing' ,
              degauss = 0.005d0 ,
             smearing = 'methfessel-paxton' ,
             vdw_corr = 'grimme-d2' ,
 /
 &ELECTRONS
        electron_maxstep = 200,
              conv_thr = 1d-07 ,
           mixing_mode = 'local-TF' ,
           mixing_beta = 0.05d0 ,
 /
 &IONS
           ion_dynamics = 'bfgs' ,
 /
CELL_PARAMETERS alat
    1.000000000    0.000000000    0.000000000
   -0.500000000    0.866025404    0.000000000
    0.000000000    0.000000000    6.531946801
ATOMIC_SPECIES
   Ag  107.86800  Ag.pbe-n-rrkjus_psl.1.0.0.UPF
ATOMIC_POSITIONS crystal
   Ag     -0.000000000   -0.000000000    0.384989560
   Ag      0.666666667    0.333333333    0.504410443
   Ag      0.333333333    0.666666667    0.620531237
   Ag      0.000000000    0.000000000    0.740069750
```

```
K_POINTS automatic
 4 4 1   0 0 0
```

Ni (111)-slab

```
&CONTROL
                title = 'Ni' ,
            calculation = 'relax' ,
           restart_mode = 'from_scratch' ,
             wf_collect = .true. ,
                outdir = '/home/madhuriya/Ag-Ni/vdW/Ni-slab/' ,
                wfcdir = '/home/madhuriya/Ag-Ni/vdW/Ni-slab/' ,
             pseudo_dir = '/opt/apps/quantum_espresso/qe-
6.1/pseudo/pslibrary.1.0.0/pbe/PSEUDOPOTENTIALS/' ,
                prefix = 'pwscf' ,
              verbosity = 'high' ,
/
&SYSTEM
                ibrav = 0,
            celldm(1) = 4.7101058806d0,
                  nat = 3,
                 ntyp = 1,
              ecutwfc = 25 ,
              ecutrho = 250 ,
            input_dft = 'pbe' ,
          occupations = 'smearing' ,
              degauss = 0.005d0 ,
             smearing = 'methfessel-paxton' ,
                nspin = 2 ,
  starting_magnetization(1) = 0.5,
             vdw_corr = 'grimme-d2' ,
/
&ELECTRONS
        electron_maxstep = 200,
             conv_thr = 1d-06 ,
          mixing_mode = 'local-TF' ,
          mixing_beta = 0.7d0 ,
/
&IONS
          ion_dynamics = 'bfgs' ,
/
CELL_PARAMETERS alat
    1.000000000    0.000000000    0.000000000
   -0.500000000    0.866025404    0.000000000
    0.000000000    0.000000000    7.279078158
ATOMIC_SPECIES
  Ni   58.69340  Ni.pbe-n-rrkjus_psl.1.0.0.UPF
ATOMIC_POSITIONS (crystal)
Ni      -0.000000000  -0.000000000   0.115255740
Ni       0.666666667   0.333333333   0.225907718
Ni       0.333333333   0.666666667   0.335026701
Ni      -0.000000000  -0.000000000   0.445513115
```

```
K_POINTS automatic
 4 4 1   0 0 0
```

Ag-Ni Interface

```
 &CONTROL
                title = 'Ag-Ni' ,
            calculation = 'relax' ,
           restart_mode = 'from_scratch' ,
               outdir = '/home/madhuriya/Ag-Ni/vdW/Ag-Ni-Interface/' ,
               wfcdir = '/home/madhuriya/Ag-Ni/vdW/Ag-Ni-Interface/' ,
            pseudo_dir = '/opt/apps/quantum_espresso/qe-
6.1/pseudo/pslibrary.1.0.0/pbe/PSEUDOPOTENTIALS/' ,
               prefix = 'pwscf' ,
             verbosity = 'high' ,
                nstep = 100 ,
 /
 &SYSTEM
                ibrav = 0,
            celldm(1) = 9.4386863722d0,
                  nat = 14,
                 ntyp = 2,
             ecutwfc = 25 ,
             ecutrho = 250 ,
            input_dft = 'pbe' ,
          occupations = 'smearing' ,
             degauss = 0.005d0 ,
            smearing = 'marzari-vanderbilt' ,
               nspin = 2 ,
  starting_magnetization(1) = 0.5,
            vdw_corr = 'grimme-d2' ,
 /
 &ELECTRONS
        scf_must_converge = .false. ,
             conv_thr = 1d-07 ,
          startingpot = 'atomic' ,
          mixing_mode = 'local-TF' ,
          mixing_beta = 0.7d0 ,
 /
 &IONS
          ion_dynamics = 'damp' ,
 /
CELL_PARAMETERS alat=
    1.000000000    0.000000000    0.000000000
   -0.500000000   -0.869428920    0.000000000
    0.000000000    0.000000000    5.913999368
ATOMIC_SPECIES
  Ag  107.86800  Ag.pbe-n-rrkjus_psl.1.0.0.UPF
  Ni   58.69340  Ni.pbe-n-rrkjus_psl.1.0.0.UPF
ATOMIC_POSITIONS crystal
  Ag      0.334246691    0.004687892    0.155136108
```

```
  Ag    -0.003690471   0.328856422   0.155151350
  Ag     0.671420995   0.666569312   0.155124138
  Ag    -0.000830205  -0.000426887   0.233762052
  Ag     0.666234612   0.333839327   0.234656523
  Ag     0.332833038   0.666865850   0.231454475
  Ni     0.331236910   0.165101677   0.311979945
  Ni     0.833831149   0.165237060   0.311973944
  Ni     0.332993883   0.665856267   0.316715589
  Ni     0.833988683   0.667963644   0.311941302
  Ni     0.165430503   0.330626206   0.380843945
  Ni     0.666970358   0.333974637   0.379272138
  Ni     0.165384584   0.835284884   0.380815767
  Ni     0.669949270   0.835563710   0.380816612
K_POINTS automatic
 4 4 1   0 0 0
```

Graphene Superlattice

```
&CONTROL
                title = 'GO' ,
          calculation = 'relax' ,
         restart_mode = 'from_scratch' ,
           wf_collect = .true. ,
               outdir = '/home/madhuriya/Ag-Ni/GO/' ,
               wfcdir = '/home/madhuriya/Ag-Ni/GO/' ,
           pseudo_dir = '/opt/apps/quantum_espresso/qe-
6.1/pseudo/pslibrary.1.0.0/pbe/PSEUDOPOTENTIALS/' ,
               prefix = 'pwscf' ,
            verbosity = 'high' ,
 /
 &SYSTEM
                ibrav = 0,
            celldm(1) = 9.9333961239d0,
                  nat = 8,
                 ntyp = 1,
              ecutwfc = 50 ,
              ecutrho = 400 ,
                 nbnd = 50,
            input_dft = 'pbe' ,
          occupations = 'smearing' ,
              degauss = 0.005d0 ,
            smearing = 'marzari-vanderbilt' ,
            vdw_corr = 'grimme-d2' ,
/
 &ELECTRONS
      electron_maxstep = 200,
             conv_thr = 1d-06 ,
         mixing_mode = 'local-TF' ,
```

```
            mixing_beta = 0.7d0 ,
 /
 &IONS
            ion_dynamics = 'bfgs'
 /
CELL_PARAMETERS alat
    1.000000000    0.000000000    0.000000000
   -0.500000000    0.866025404    0.000000000
    0.000000000    0.000000000    1.909176510
ATOMIC_SPECIES
   C   12.01070  C.pbe-n-rrkjus_psl.1.0.0.UPF
ATOMIC_POSITIONS crystal
   C      0.333700887    0.184686245    0.588347888
   C      0.833828241    0.184740171    0.588327913
   C      0.167059375    0.351339991    0.588321870
   C      0.667076192    0.351300916    0.588327069
   C      0.333654895    0.684633366    0.588332772
   C      0.833832636    0.684557864    0.588299815
   C      0.167079247    0.851343793    0.588302468
   C      0.667148522    0.851272881    0.588340545
K_POINTS automatic
  4 4 1   0 0 0
```

Ag-Ni-graphene Superlattice

```
&CONTROL
            calculation = 'relax' ,
           restart_mode = 'from_scratch' ,
                outdir = '/home/madhuriya/Ag-Ni/vdW/Ag-Ni-GO-Interface/' ,
                wfcdir = '/home/madhuriya/Ag-Ni/vdW/Ag-Ni-GO-Interface/' ,
             pseudo_dir = '/opt/apps/quantum_espresso/qe-
6.1/pseudo/pslibrary.1.0.0/pbe/PSEUDOPOTENTIALS/' ,
                prefix = 'pwscf' ,
              verbosity = 'high' ,
                 nstep = 200 ,
 /
 &SYSTEM
                 ibrav = 0,
              celldm(1) = 15.6115872596d0,
                   nat = 22,
                  ntyp = 3,
               ecutwfc = 25 ,
               ecutrho = 250 ,
              input_dft = 'pbe' ,
            occupations = 'smearing' ,
               degauss = 0.005d0 ,
              smearing = 'marzari-vanderbilt' ,
                 nspin = 2 ,
  starting_magnetization(1) = 0.5,
              vdw_corr = 'grimme-d2' ,
```

```
 /
 &ELECTRONS
              startingpot = 'atomic' ,
              startingwfc = 'atomic' ,
              mixing_mode = 'local-TF' ,
              mixing_beta = 0.7 ,
 /
 &IONS
             ion_dynamics = 'bfgs' ,
                          ion_positions = 'default' ,
          trust_radius_min = 0.1 ,
 /
CELL_PARAMETERS alat
     1.000000000    0.000000000    0.000000000
    -0.500000000   -0.869428920    0.000000000
     0.000000000    0.000000000    3.071492989
ATOMIC_SPECIES
   Ag  107.86800  Ag.pbe-n-rrkjus_psl.1.0.0.UPF
    C   12.01070  C.pbe-n-rrkjus_psl.1.0.0.UPF
   Ni   58.69340  Ni.pbe-n-rrkjus_psl.1.0.0.UPF
ATOMIC_POSITIONS crystal
   Ag      0.482591405    0.095672042    0.224743330
   Ag      0.465961102    0.062649592    0.334183136
   Ag      0.831479001    0.246635872    0.276415281
   Ag      0.236669756    0.213712724    0.221211112
   Ag      0.588497593    0.400035102    0.162630853
   Ag      0.591309921    0.406810990    0.277998346
   Ni      0.580536144    0.664930848    0.222655145
   Ni      0.752406341    0.756524723    0.303370193
   Ni      0.416089494    0.588398347    0.302843962
   Ni      0.228387741    0.509982114    0.223294427
   Ni      0.582722583    0.892401734    0.275252982
   Ni      0.067298847    0.658065284    0.194879935
   Ni      0.399651617    0.792505391    0.185373272
   Ni      0.243059066    0.749696117    0.273926238
    C      0.704727396    0.619903418    0.049289043
    C      0.610324761    0.710564696    0.048957847
    C      0.325862383    0.425816647    0.048880519
    C      0.616529369    0.420547169    0.049633459
    C      0.415994403    0.331492447    0.049210889
    C      0.411109831    0.624209457    0.049273478
    C      0.317922411    0.719576935    0.050339693
    C      0.710288943    0.324958605    0.050288225
K_POINTS automatic
  4 4 1   0 0 0
```

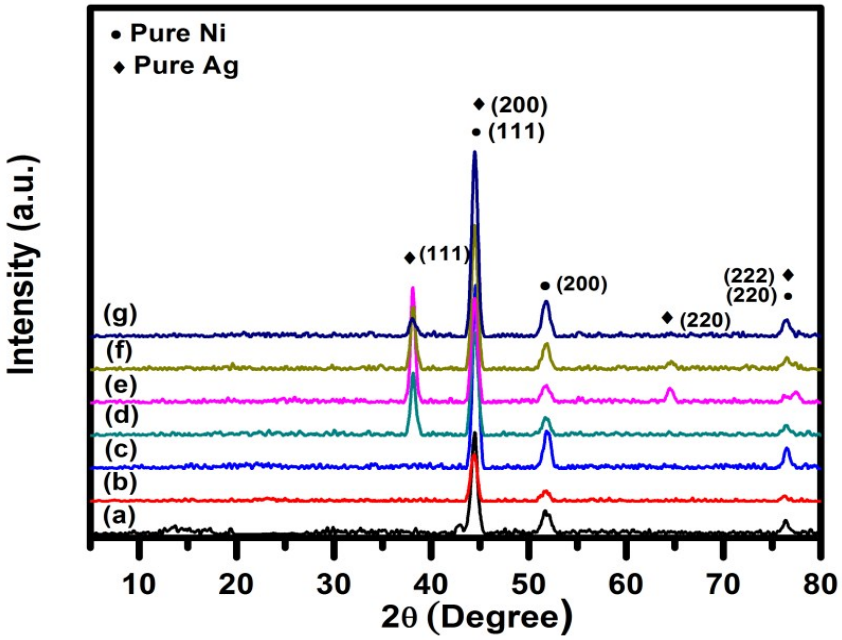

Fig. S1. Room temperature wide angle powder XRD pattern of (a) $Ni_{10}RGO_{90}$, (b) $Ni_{20}RGO_{80}$, (c) $Ni_{40}RGO_{60}$, (d) $Ag_{0.05}Ni_{0.95}$, (e) $Ag_{0.15}Ni_{0.85}$, (f) $Ag_{0.25}Ni_{0.75}$, and (g) $Ag_{0.27}Ni_{0.73}$.

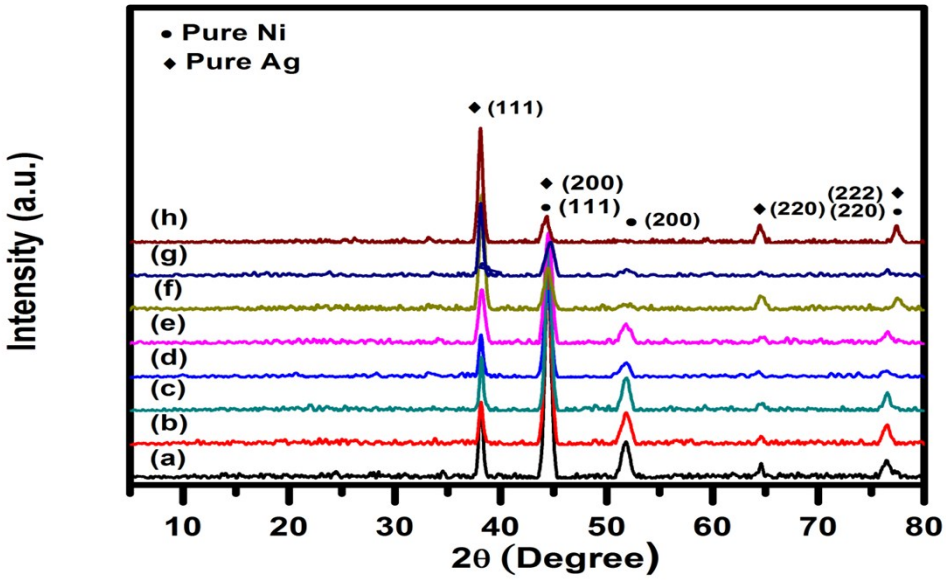

Fig. S2. Room temperature wide angle powder XRD pattern of (a) $(Ag_{0.05}Ni_{0.95})_{90}RGO_{10}$, (b) $(Ag_{0.05}Ni_{0.95})_{70}RGO_{30}$, (c) $(Ag_{0.05}Ni_{0.95})_{60}RGO_{40}$, (d) $(Ag_{0.05}Ni_{0.95})_{50}RGO_{50}$, (e) $(Ag_{0.05}Ni_{0.95})_{40}RGO_{60}$, (f) $(Ag_{0.15}Ni_{0.85})_{33.5}RGO_{66.5}$, (g) $(Ag_{0.37}Ni_{0.63})_{40.5}RGO_{59.5}$, and (h) $(Ag_{0.45}Ni_{0.55})_{44}RGO_{56}$.

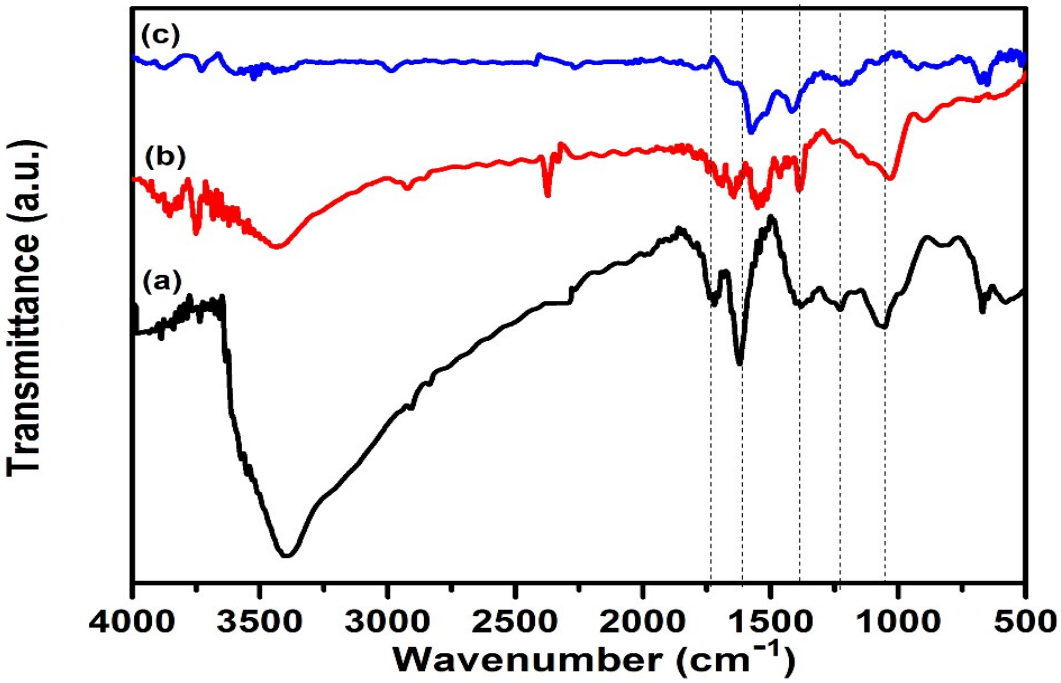

Fig. S3. FT-IR spectra of (a) GO, (b) RGO, and (c) $(Ag_{0.27}Ni_{0.73})_{37}RGO_{63}$ nanocomposite.

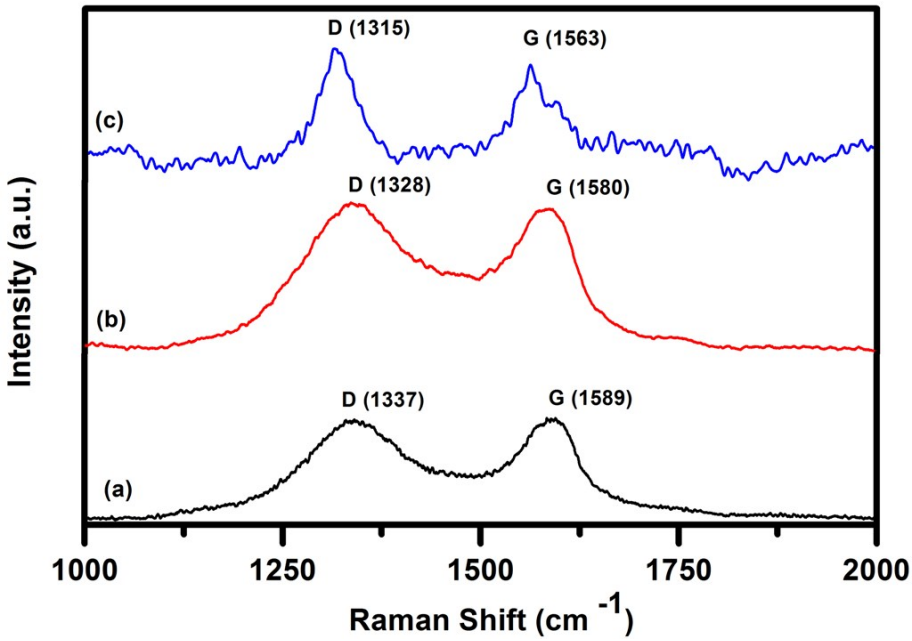

Fig. S4. Raman spectra of (a) GO, (b) RGO, and (c) $(Ag_{0.27}Ni_{0.73})_{37}RGO_{63}$ nanocomposite.

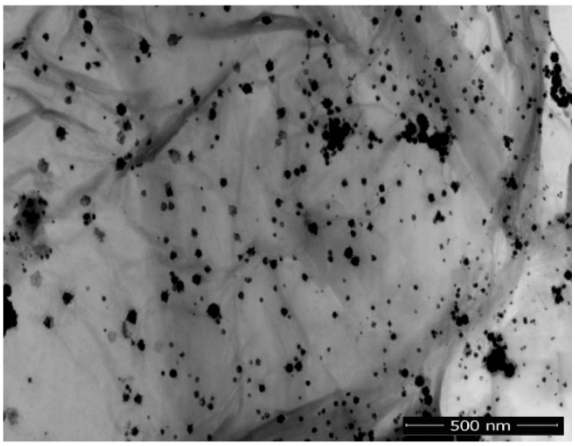

Fig. S5. STEM image of synthesized $(Ag_{0.27}Ni_{0.73})_{37}RGO_{63}$ nanocomposite.

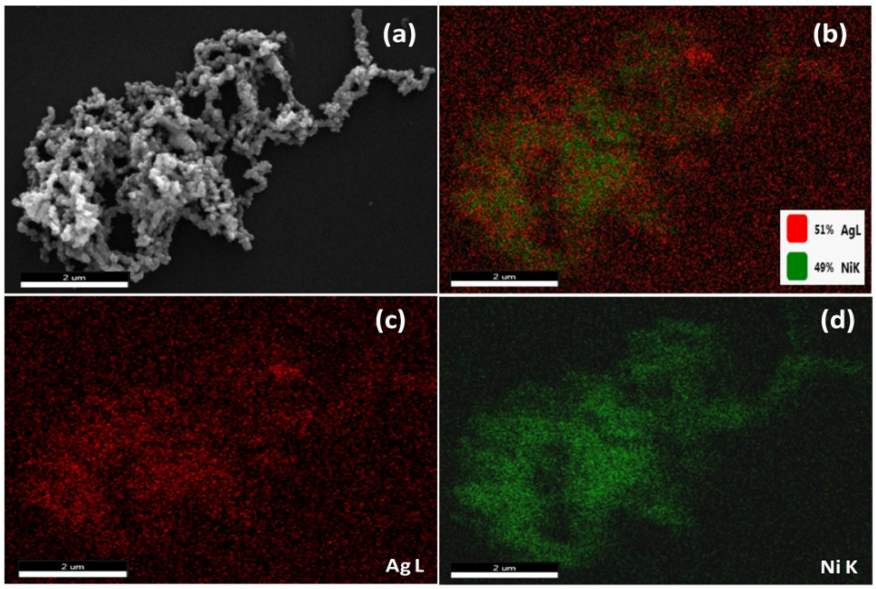

Fig. S6. (a) FESEM micrographs and (b-d) elemental color mapping of synthesized $Ag_{0.50}Ni_{0.50}$ nanocomposite.

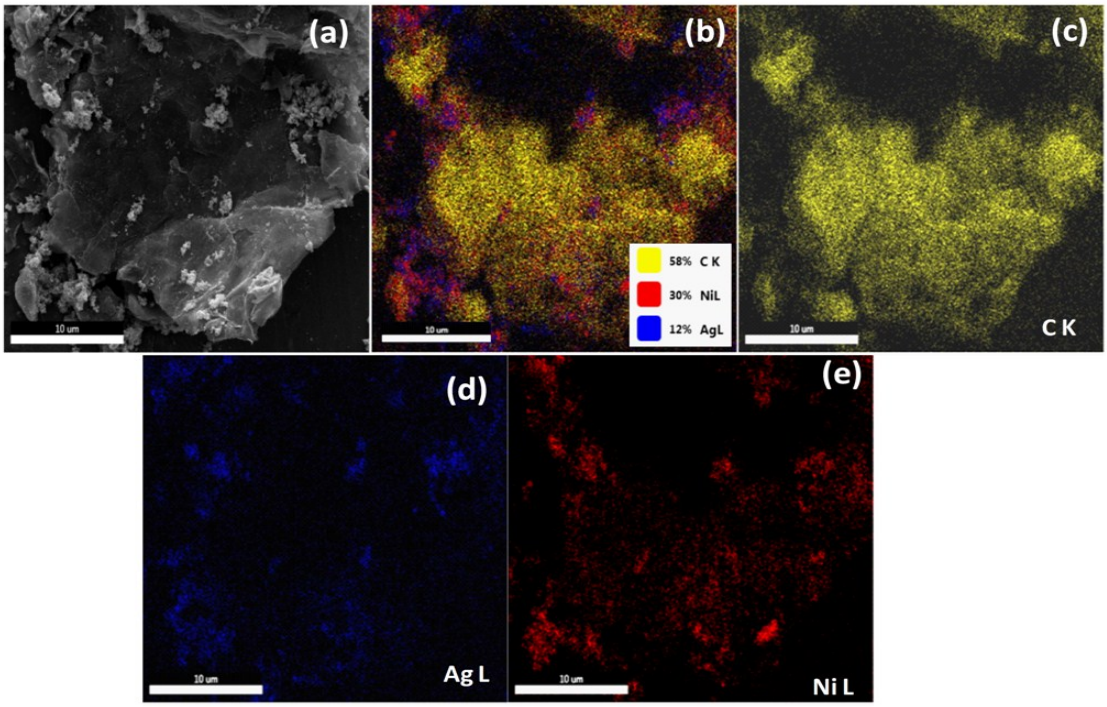

Fig. S7. (a) FESEM micrographs and (b-e) elemental color mapping of synthesized $(Ag_{0.27}Ni_{0.73})_{37}RGO_{63}$ nanocomposite.

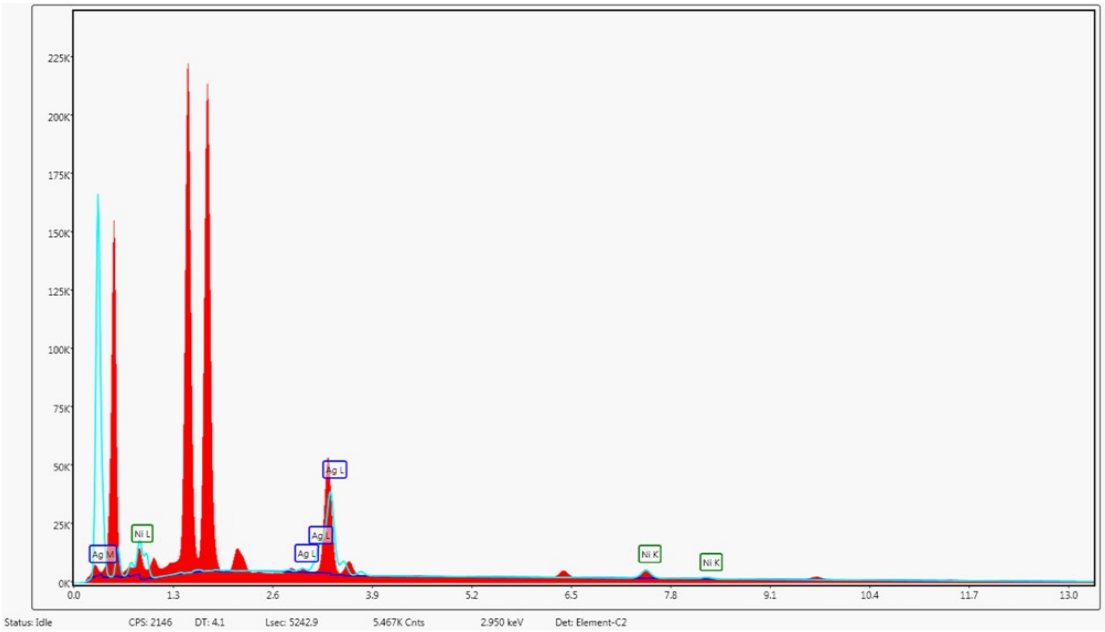

Fig. S8. EDS spectra of synthesized $Ag_{0.50}Ni_{0.50}$ nanocomposite

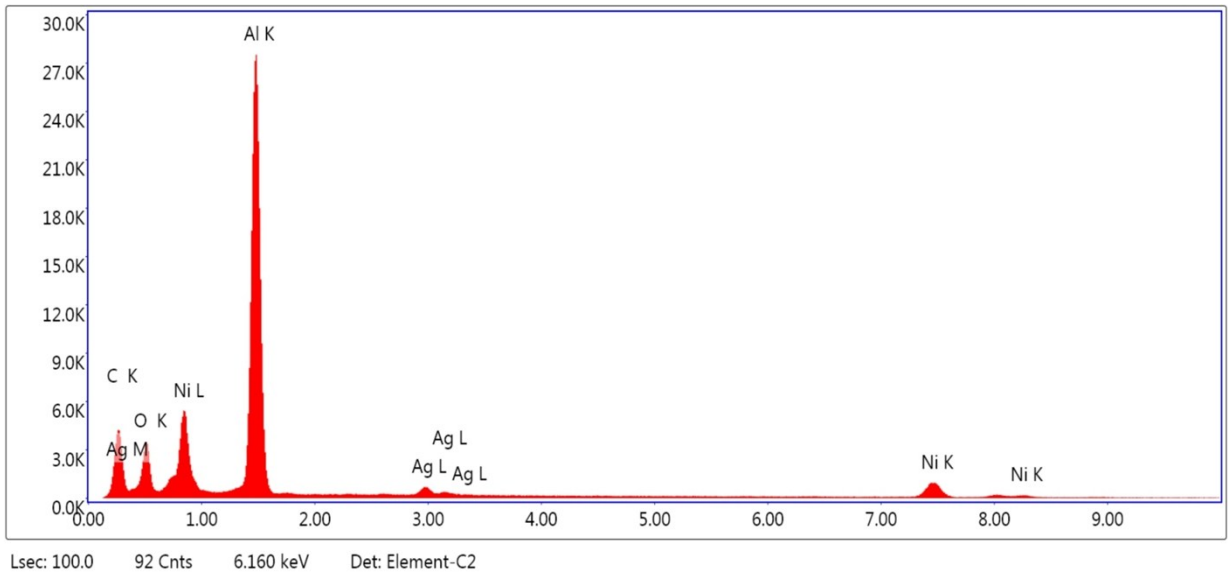

Fig. S9. EDS spectra of synthesized $(Ag_{0.27}Ni_{0.73})_{37}RGO_{63}$ nanocomposite.

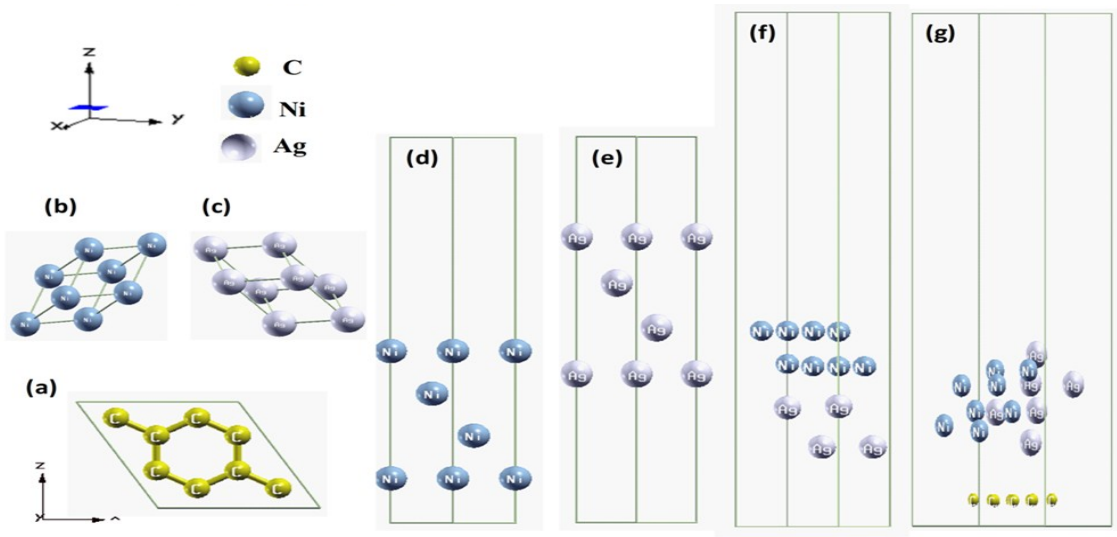

Fig. S10. The initial structure of (a) graphene superlattice, (b) Ni unitcell, (c) Ag unitcell (d) Ni (111) slab, (e) Ag (111) slab, (f) Ag-Ni Interface, and (d) Ag-Ni-graphene superlattice.

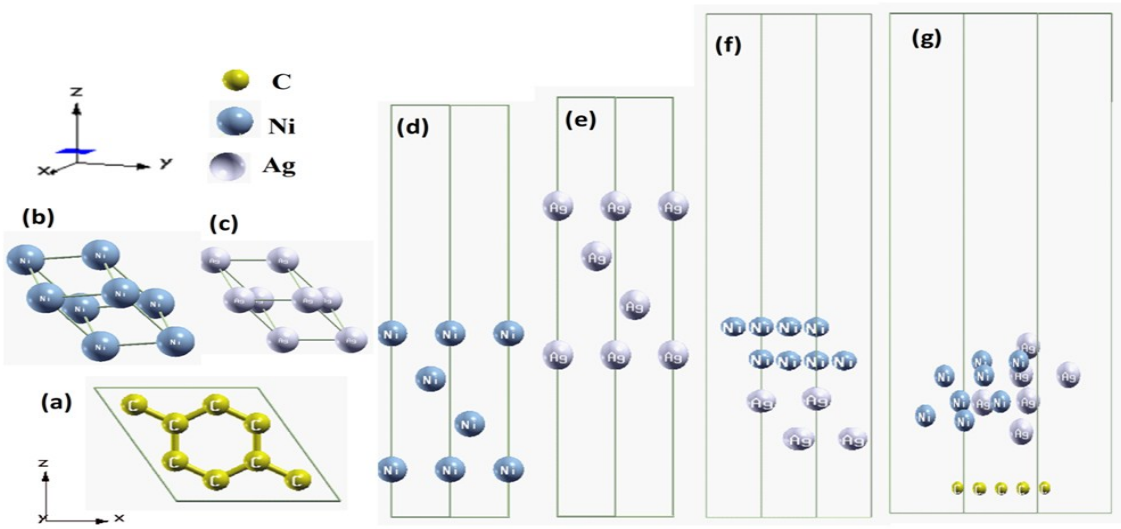

Fig. S11. The optimized structure of (a) graphene superlattice, (b) Ni unitcell, (c) Ag unitcell (d) Ni (111) slab, (e) Ag (111) slab, (f) Ag-Ni Interface, and (d) Ag-Ni-graphene superlattice.

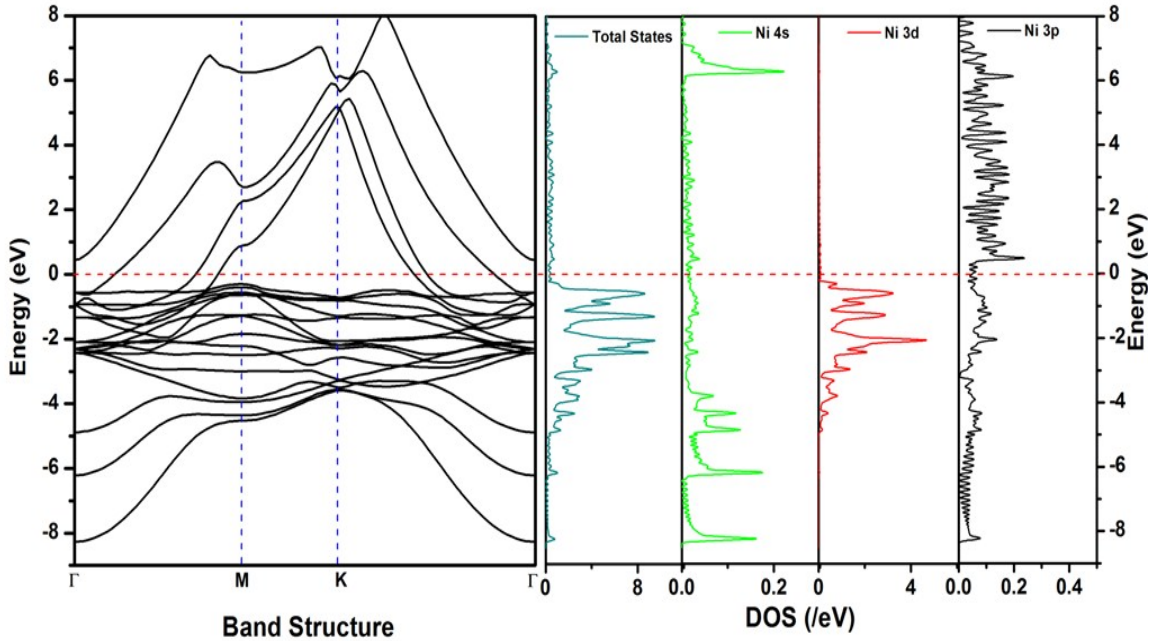

Fig. S12. The band structure and density of states of Ni (111) slab spin up.

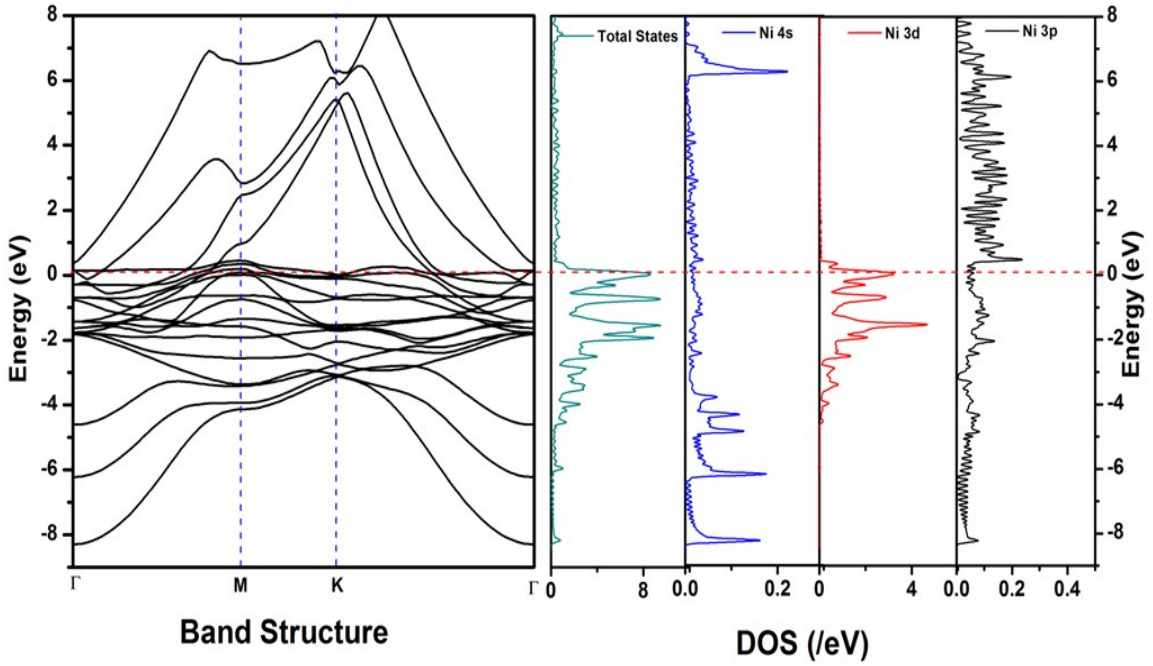

Fig. S13. The band structure and density of states of Ni (111) slab spin down.

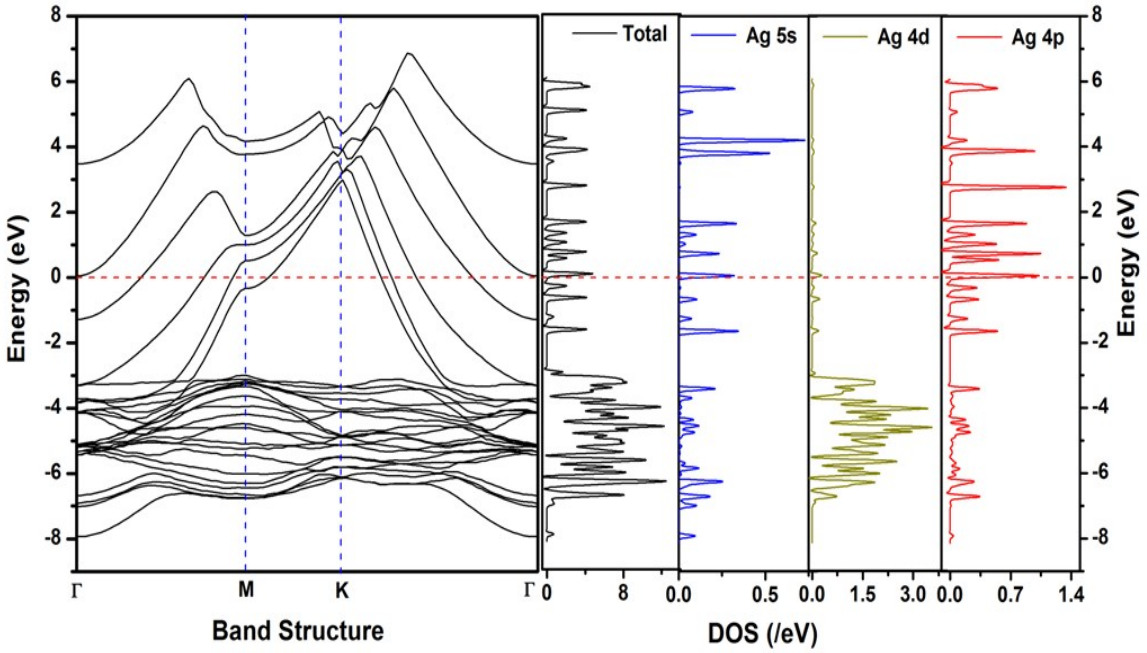

Fig. S14. The band structure and density of states of Ag (111) slab.

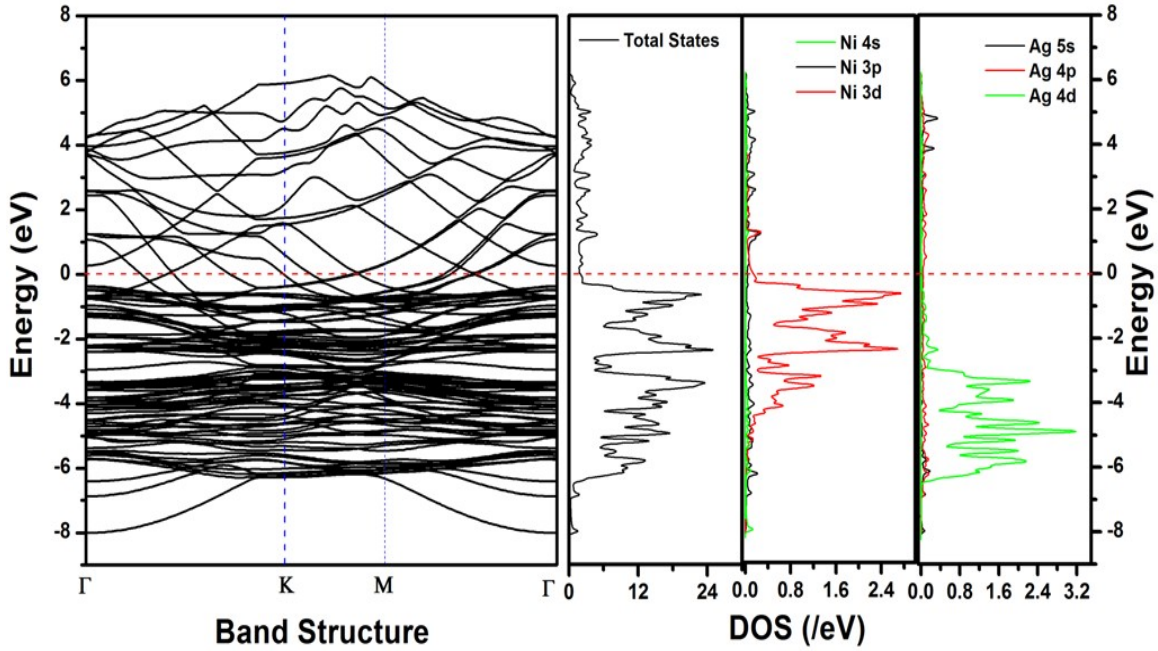

Fig. S15. The band structure and density of states of Ag-Ni interface spin up.

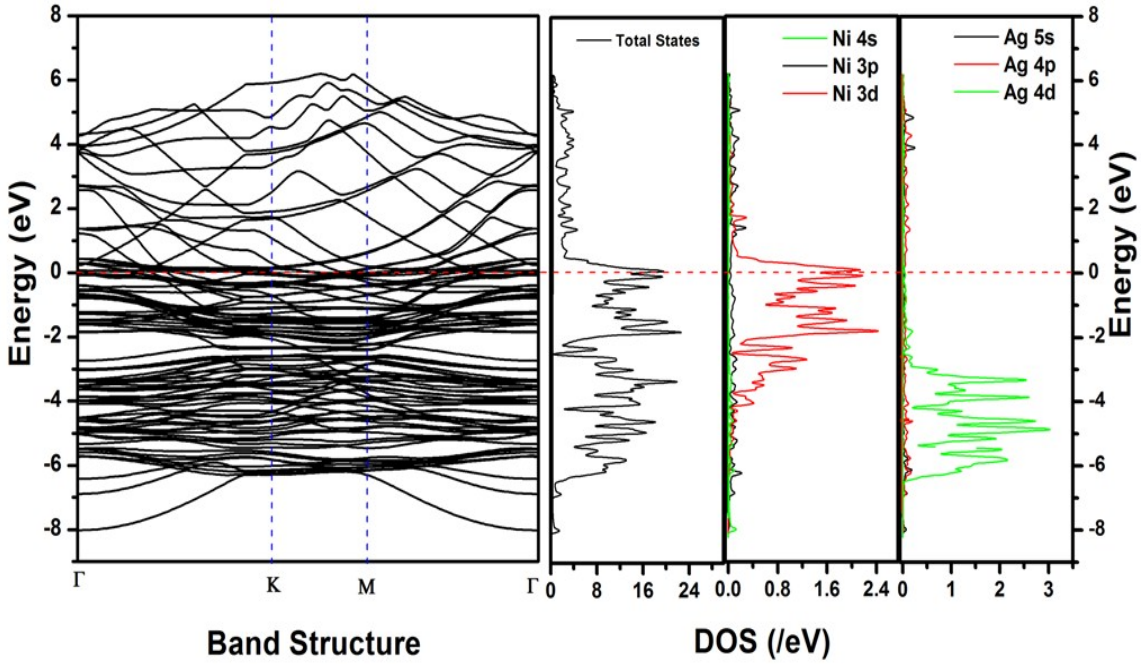

Fig. S16. The band structure and density of states of Ag-Ni interface spin down.

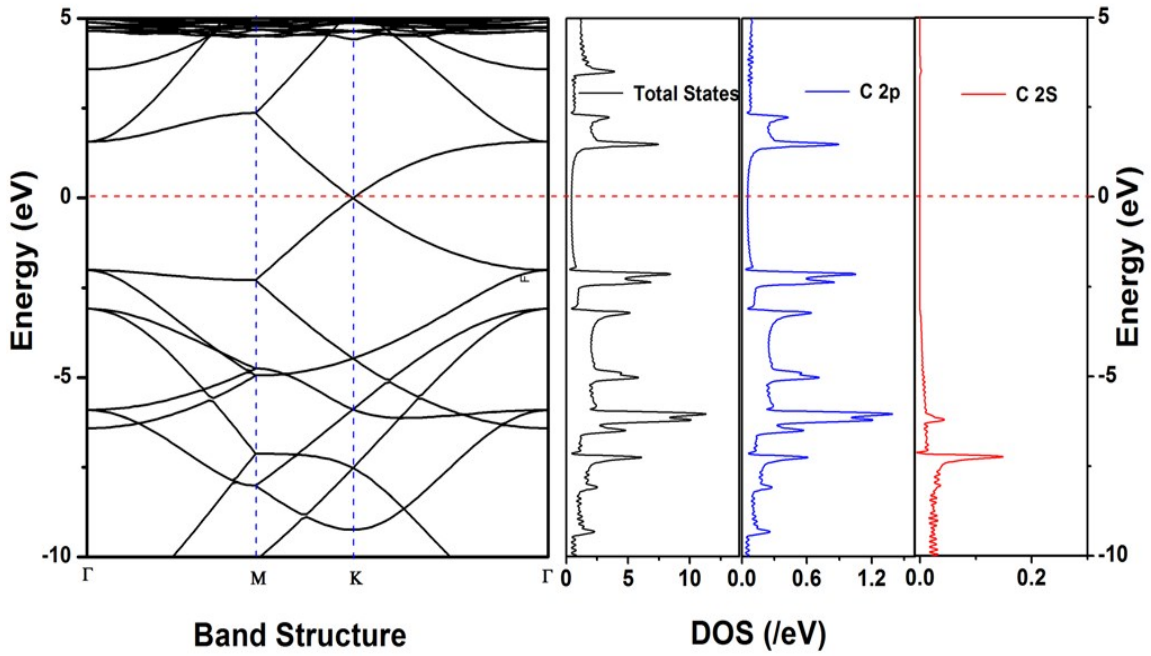

Fig. S17. The band structure and density of states of graphene superlattice.

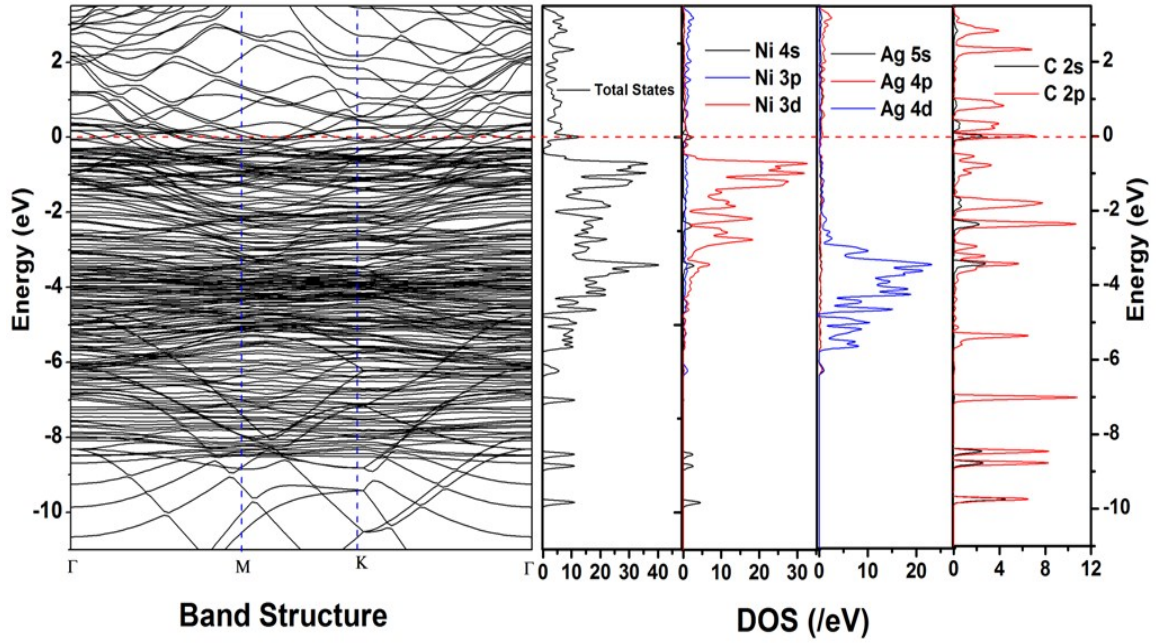

Fig. S18. The band structure and density of states of Ag-Ni-graphene superlattice spin up.

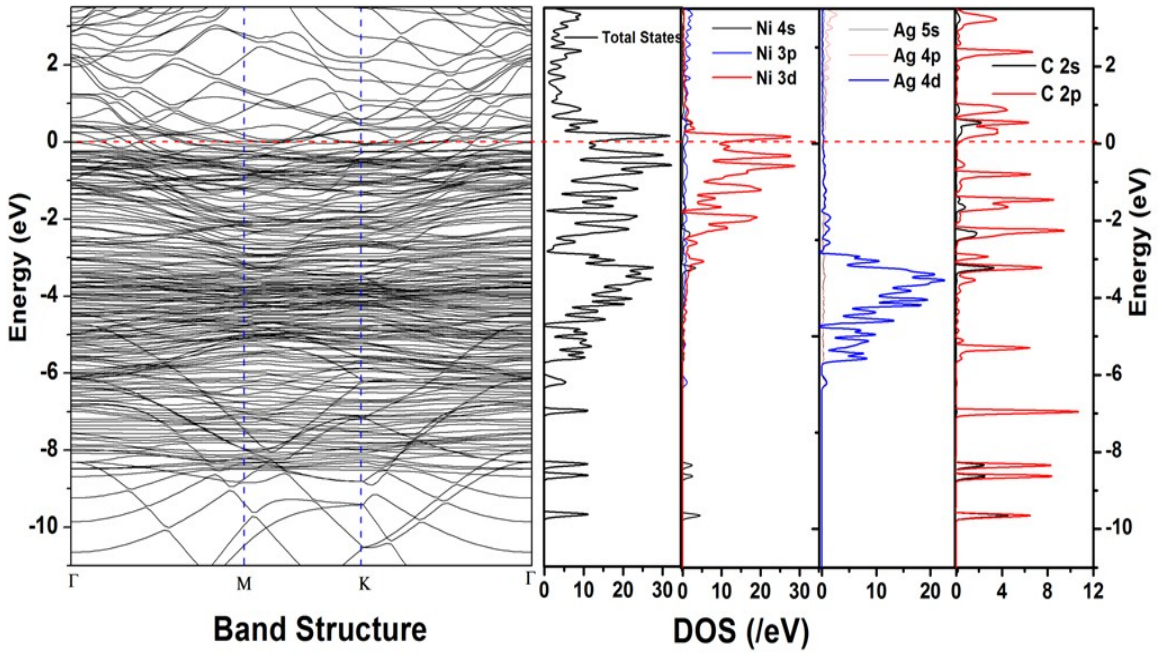

Fig. S19. The band structure and density of states of Ag-Ni-graphene superlattice spin down.

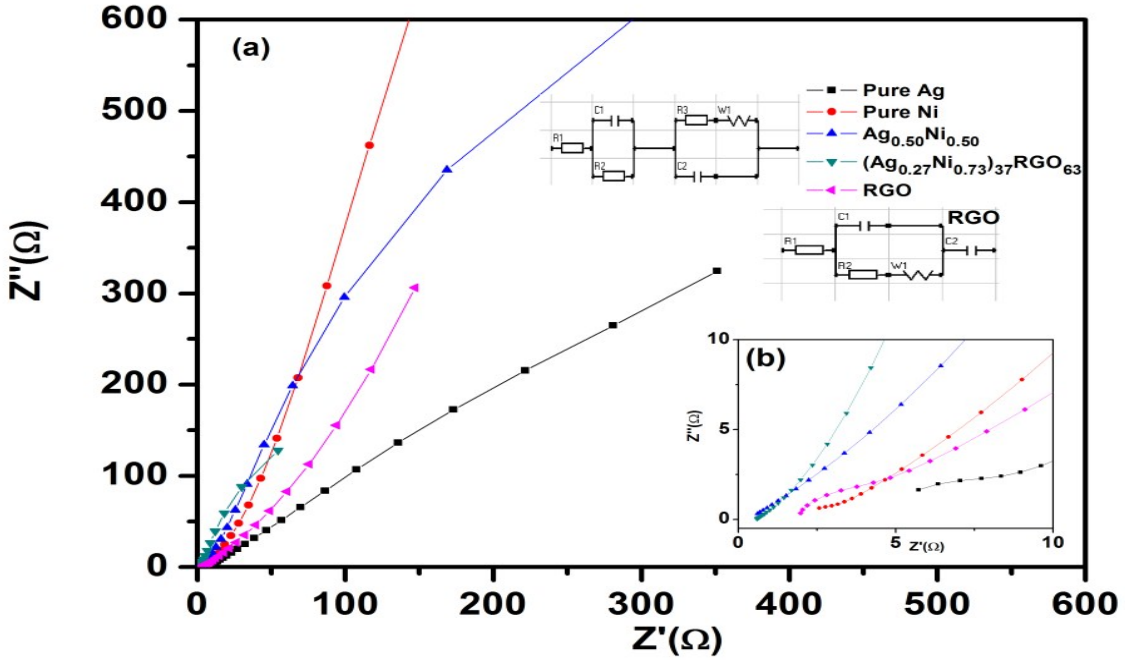

Fig. S20. (a) Electrochemical impedance spectra of Pure Ni, Pure Ag, $Ag_{0.50}Ni_{0.50}$, $(Ag_{0.27}Ni_{0.73})_{37}RGO_{63}$ and RGO (b) Inset shows the high frequency region of the impedance spectra and equivalent circuit used for fitting the Nyquist plots.

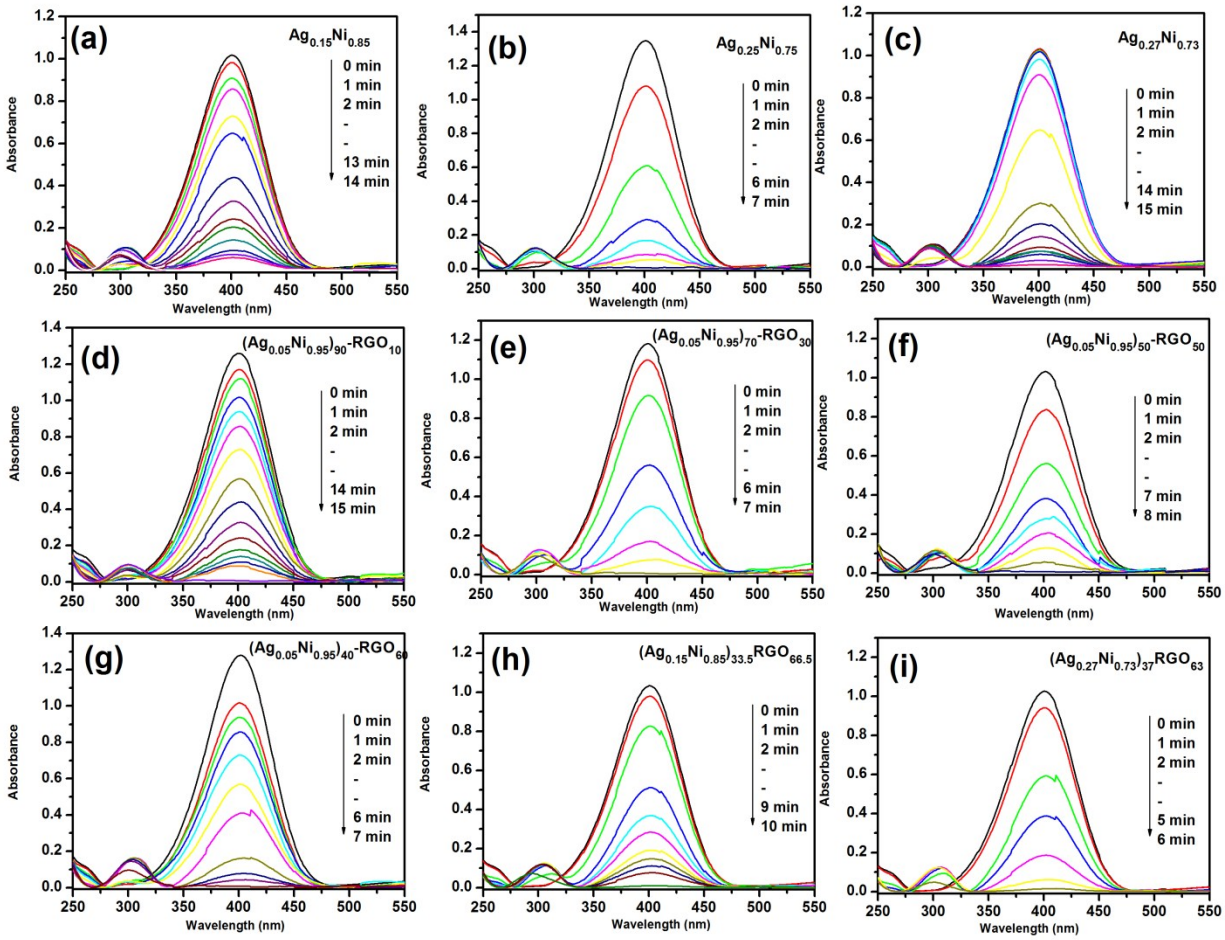

Fig. S21. Time dependent UV-Vis spectral changes of the reaction mixture of 4-NP catalyzed by (a) $Ag_{0.15}Ni_{0.85}$, (b) $Ag_{0.25}Ni_{0.75}$, (c) $Ag_{0.27}Ni_{0.73}$, (d) $(Ag_{0.05}Ni_{0.95})_{90}RGO_{10}$, (e) $(Ag_{0.05}Ni_{0.95})_{70}RGO_{30}$, (f) $(Ag_{0.05}Ni_{0.95})_{50}RGO_{50}$, (g) $(Ag_{0.05}Ni_{0.95})_{40}RGO_{60}$, (h) $(Ag_{0.15}Ni_{0.85})_{33.5}RGO_{66.5}$, and (i) $(Ag_{0.27}Ni_{0.73})_{37}RGO_{63}$.

Table S3. Comparison of catalytic efficiency of different reported catalysts for the reduction reaction of 4-NP in presence of $NaBH_4$.

Catalyst	Rate Constant (K_{app})	Reference
Au nanoparticle	9.19×10^{-3} s^{-1}	[4]
Ag nanoparticle	4.06×10^{-3} s^{-1}	[4]
Cu nanoparticle	1.5×10^{-3} s^{-1}	[5]
AgNP-PG-5K	$5.5\times10^{-3}s^{-1}$	[6]
AgNP@PGMA-SH	$3.94\times10^{-3}s^{-1}$	[7]
Ag nanoparticles	$1.26\times10^{-3}s^{-1}$	[8]
Ag NPs with PAA stabilizer	$15.46\times10^{-3}s^{-1}$	[9]
Ni Nps	$5.45\times10^{-3}s^{-1}$	[10]
Ag monometallic	$5.1\times10^{-3}s^{-1}$	[11]
Ni monometallic	$3.7\times10^{-3}s^{-1}$	[11]
Ni NPs	2.7×10^{-3} s^{-1}	[12]
RANEY Ni	$3.2\times10^{-3}s^{-1}$	[12]
Ni NPs	1.4×10^{-3} s^{-1}	[13]
Ni-NPs composite brushes	1.0×10^{-3} s^{-1}	[14]
Pd-Ag	$39.1\times10^{-3}s^{-1}$	[15]
Au-Ag	$13.3\times10^{-3}s^{-1}$	[16]
$Au_{0.1}Ag_{0.9}$	$3.8\times10^{-3}s^{-1}$	[17]
Bare $Ag_{50}Ni_{50}$	6.07×10^{-3} s^{-1}	[18]
$Ag_{0.6}Ni_{0.4}$	$32.2\times10^{-3}s^{-1}$	[19]
Ni/Ag	$2.16\times10^{-3}s^{-1}$	[20]
Ni-Ag bimetallic	$5.6\times10^{-3}s^{-1}$	[11]
Ni-RGO	1.8×10^{-3} s^{-1}	[21]
Ni/RGO	14.82×10^{-3} s^{-1}	[22]
Ni/RGO	11.7×10^{-3} s^{-1}	[10]
Ni-CNF	$92.0\times10^{-3}s^{-1}$	[23]
Ni@RGO	$12.8\times10^{-3}s^{-1}$	[11]
Ag-NP/C composite	$1.69\times10^{-3}s^{-1}$	[24]
Ag-RGO	$0.0006\times10^{-3}s^{-1}$	[25]
Ag-KCC	$0.10\times10^{-3}s^{-1}$	[26]

Ag/PAN	$0.20\times10^{-3}s^{-1}$	[27]
PANI/Ag	$0.256\times10^{-3}s^{-1}$	[28]
RGONS/Ag-NSs	$0.535\times10^{-3}s^{-1}$	[29]
Ag/CNF	$90.5\times10^{-3}s^{-1}$	[23]
Ni-Ag@RGO	$89\times10^{-3}\ s^{-1}$	[11]
Ag-Au/rGO	$3.47\times10^{-3}\ s^{-1}$	[30]
$CuO_{0.05}$ –rGO	$231\times10^{-3}\ s^{-1}$	[31]
RGO-$Ni_{25}Co_{75}$	$93.22\times10^{-3}s^{-1}$	[32]
RGO-$ZnNi_5$-2	$3.92\times10^{-3}s^{-1}$	[33]
$Ag_{50}Ni_{50}$/RGO	$48.4\times10^{-3}\ s^{-1}$	[18]
Au_1-Cu_3/rGO	$96\times10^{-3}\ s^{-1}$	[34]
Fe_3O_4/graphene/Pt	$20.0\times10^{-3}\ s^{-1}$	[35]
Fe_3O_4/graphene/Pd	$61.0\times10^{-3}s^{-1}$	[35]
Au/graphene hydrogel	$3.17\times10^{-3}\ s^{-1}$	[36]
Ag@Fe_3O_4@C Core shell	$17.1\ \times10^{-3}\ s^{-1}$	[37]
PtNi nanosnowflakes/RGO	$2.17\times10^{-3}\ s^{-1}$	[38]
Ag@SBA-15	$1.7\times10^{-3}\ s^{-1}$	[39]
2.5Ru@SBA-15	$13.5\times10^{-3}\ s^{-1}$	[40]
Pure Ni	$2.46\ \times10^{-3}\ s^{-1}$	This work
Pure Ag	$10.32\ \times10^{-3}\ s^{-1}$	This work
$Ni_{40}RGO_{60}$	$6.66\ \times10^{-3}\ s^{-1}$	This work
$Ag_{0.05}Ni_{0.95}$	$1.50\ \times10^{-3}\ s^{-1}$	This work
$(Ag_{0.05}Ni_{0.95})_{60}RGO_{40}$	$19.60\ \times10^{-3}\ s^{-1}$	This work

A3 coupling reaction

Table S4. Catalytic performance of the as-prepared catalysts for synthesis of N,N-diethyl-3-phenylprop-2-yn-1-amine.

Catalyst	Yield (%)
Pure Ni	71
Pure Ag	79
$Ni_{10}RGO_{90}$	43
$Ni_{20}RGO_{80}$	67
$Ni_{30}RGO_{70}$	80
$Ag_{0.50}Ni_{0.50}$	85
$(Ag_{0.15}Ni_{0.85})_{33.5}RGO_{66.5}$	90
$(Ag_{0.27}Ni_{0.73})_{37}RGO_{63}$	95
$(Ag_{0.37}Ni_{0.63})_{40.5}RGO_{59.5}$	95
$(Ag_{0.45}Ni_{0.55})_{44}RGO_{56}$	96

[a]**Reaction condition :** Paraformaldehyde (2mmol), Diethylamine (2.4mmol), Phenylacetylene (3 mmol), Catalyst amount 50 mg, Acetonitrile 10 ml, Reaction temperature 100 ^{o}C, reaction time 12 h

Table S5. Synthesis of N,N-diethyl-3-phenylprop-2-yn-1-amine under various reaction conditions in the presence of $(Ag_{0.27}Ni_{0.73})_{37}RGO_{63}$[a].

Reaction Temperature (°C)	Reaction Time (h)	Catalyst Amount (mg)	Solvent	Yield (%)
100°C	12	25	Acetonitrile	58
100°C	12	50	Acetonitrile	95
100°C	12	75	Acetonitrile	92
100°C	12	50	Dichloromethane	56
100°C	12	50	Chloroform	52
100°C	12	50	Methanol	37
100°C	12	50	Toluene	45
100°C	12	50	Water	15
60°C	12	50	Acetonitrile	47
80°C	12	50	Acetonitrile	63

120°C	12	50	Acetonitrile	82

[a]**Reaction condition :** Paraformaldehyde (2mmol), Diethylamine (2.4mmol), Phenylacetylene (3 mmol), Catalyst $(Ag_{0.27}Ni_{0.73})_{37}RGO_{63}$, solvent 10 ml

Table S6. Comparison of the catalytic efficiency of $(Ag_{0.27}Ni_{0.73})_{37}RGO_{63}$ with different reported catalysts for the synthesis of N,N-diethyl-3-phenylprop-2-yn-1-amine via A3 coupling reaction.

Catalyst	Solvent	Time	% of Yield	Reference
Ag/diatomite	Toluene	24 h	82	[41]
Ag_2O/alumina	water	2 h	92	[42]
Ag/SBA-15-6	Glycol	30 min	95	[43]
H-Fe_2O_3@DA/Ag	-	40 min	90	[44]
Au/ZrO_2	Dioxane	6 h	90	[45]
$(Ag_{0.27}Ni_{0.73})_{37}RGO_{63}$	Acetonitrile	12 h	95	Present work

Styrene Epoxidation reaction

Table S7. Effect of catalyst composition on the percentage of styrene conversion and percentage of selectivity of styrene oxide and benzaldehyde formation.

Catalyst	Conversion (%)	Selectivity	
		Styrene Oxide (%)	PhCHO (%)
Pure Ni	69	85	5
Pure Ag	76	88	4

$Ni_{30}RGO_{70}$	78	89	4
$Ag_{0.50}Ni_{0.50}$	81	86	3
$(Ag_{0.15}Ni_{0.85})_{33.5}RGO_{66.5}$	84	89	6
$(Ag_{0.27}Ni_{0.73})_{37}RGO_{63}$	96	89	4
$(Ag_{0.37}Ni_{0.63})_{40.5}RGO_{59.5}$	89	82	5
$(Ag_{0.45}Ni_{0.55})_{44}RGO_{56}$	88	79	5

Reaction condition : Styrene (5 mmol), TBHP (12.5 mmol), Acetonitrile (4 ml), Reaction time = 10 h , Reaction temperature = 100 °C, catalyst amount = 25 mg

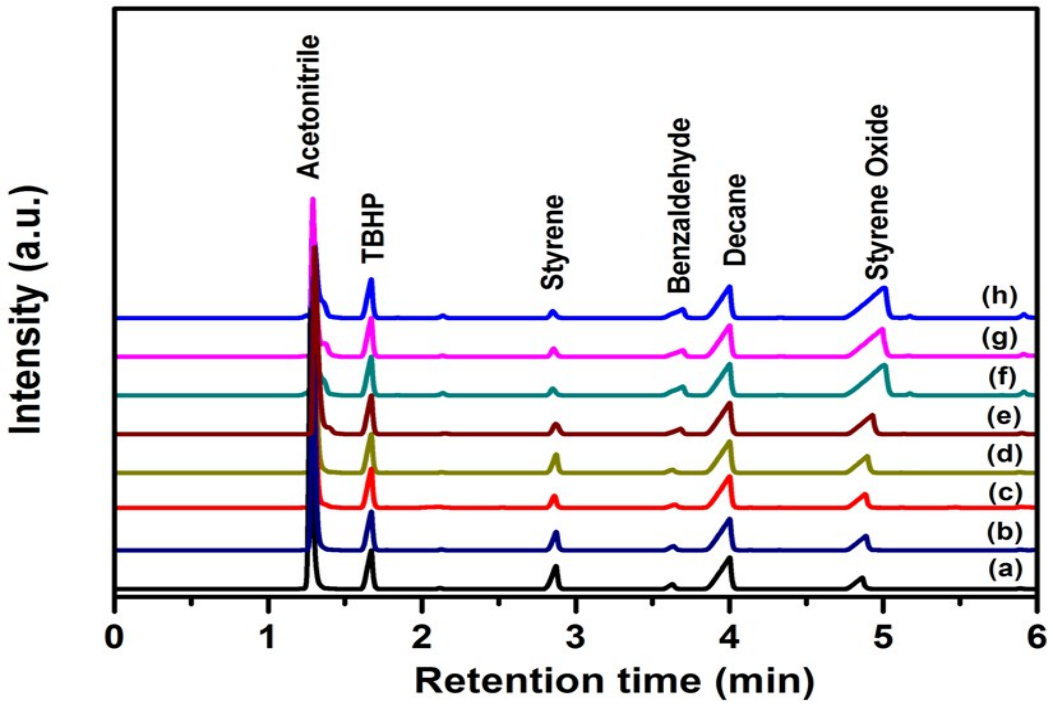

Fig. S22. Gas chromatography analysis of styrene epoxidation reaction with (a) Pure Ni, (b) $Ni_{30}RGO_{70}$, (c) Pure Ag, (d) $Ag_{0.50}Ni_{0.50}$, (e) $(Ag_{0.15}Ni_{0.85})_{33.5}RGO_{66.5}$, (f) $(Ag_{0.27}Ni_{0.73})_{37}RGO_{63}$, (g) $(Ag_{0.37}Ni_{0.63})_{40.5}RGO_{59.5}$, and (h) $(Ag_{0.45}Ni_{0.55})_{44}RGO_{56}$.

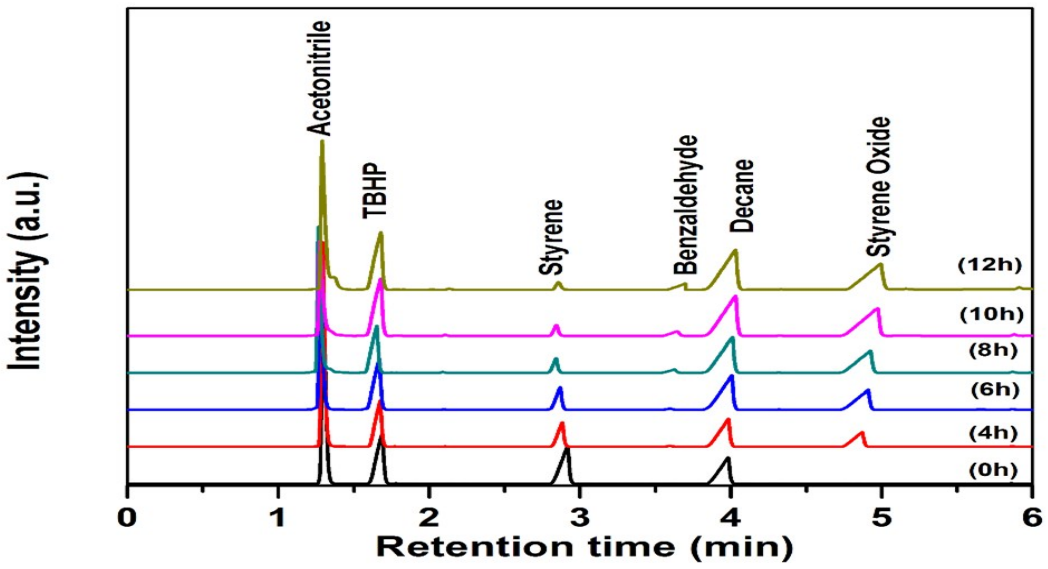

Fig. S23. Gas chromatography analysis of progress of $(Ag_{0.27}Ni_{0.73})_{37}RGO_{63}$ catalyzed styrene epoxidation reaction with time.

Table S8. Epoxidation of styrene under various reaction condition in the presence of the $(Ag_{0.27}Ni_{0.73})_{37}RGO_{63}$.

Reaction Temperature (°C)	Reaction Time (hours)	Catalyst Amount (mg)	Styrene : TBHP molar ratio	Conversion (%)	Selectivity	
					Styrene Oxide (%)	PhCHO (%)
80°C	10	25	1:2	67	57	11
100°C	10	25	1:2	95	87	4
120°C	10	25	1:2	79	89	9
100°C	10	10	1:2	65	69	6
100°C	10	50	1:2	94	74	7
100°C	10	25	1:1	39	49	8
100°C	10	25	1:1.5	69	80	4
100°C	10	25	1:2.5	93	79	9
100°C	10	25	1:3.0	94	69	6
100°C	4	25	1:2.0	35	96	3
100°C	6	25	1:2.0	50	94	3

100°C	8	25	1:2.0	73	91	4
100°C	12	25	1:2.0	96	82	7

Reaction condition : Styrene, TBHP, Acetonitrile (4 ml), catalyst amount = 25 mg

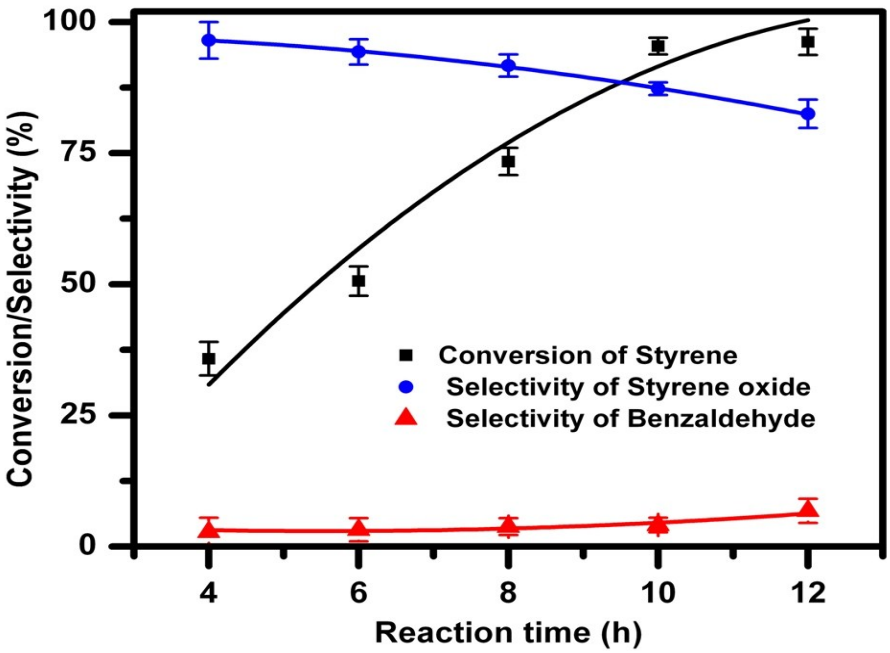

Fig. S24. Change of conversion and product selectivity with time catalyzed by $(Ag_{0.27}Ni_{0.73})_{37}RGO_{63}$ for epoxidation of styrene. Reaction condition : 5 mmol of Styrene, 12.5 mmol of TBHP were stirred in 4 ml Acetonitrile for 12 h at 100 °C using 25 mg catalyst.

Table S9. Comparison of the catalytic efficiency of $(Ag_{0.27}Ni_{0.73})_{37}RGO_{63}$ with different reported catalysts for epoxidation reaction of styrene.

Catalyst	Solvent	Time	Styrene Conversion/ Yield %	Selectivity of Styrene oxide formation	Reference
Ag-Fe_3O_4	Toluene	13 h	100	84	[46]
Ag-$Ni_{0.81}Fe_{2.19}O_4$	Toluene	5 h	69.8	84.8	[47]
Ag-γ-ZrP	Acetonitrile	8 h	44.7	92.9	[48]
AgNps/CNFs(1/10)	Isopropanol	8 h	43.4	38.9	[49]
Ag CNFs	Acetonitrile	6 h	61.4	81.5	[50]
Ag–Cu/Cu_2O CNFs	Acetonitrile	6 h	99	41.9	[50]
Ag/SBA-15	Acetonitrile	9 h	77.7	73.7	[51]
Ag/LDH	Acetonitrile	8 h	80.8	91.1	[52]
Ag/4A Zeolite	Acetonitrile	48 h	80.8	89.2	[53]
TiO_2-Ag	Toluene	14 h	83.9	66.8	[54]
TiO_2-GO	Acetonitrile	12 h	93.3	85.9	[55]
$(Ag_{0.27}Ni_{0.73})_{37}RGO_{63}$	Acetonitrile	10 h	95	87	Present work

Click Reaction

Table S10. Comparison of the catalytic efficiency of $(Ag_{0.27}Ni_{0.73})_{37}RGO_{63}$ with different reported catalysts in the preparation of 2-phenyl-2-(4-phenyl-1H-1,2,3-triazole-1-yl) ethanol via Click reaction.

Catalyst	Solvent	Time	% of Yield	Reference
Cu^{II}-hydrotalcite	Water	5 h	91	[56]
Cu^{II}-PhTPY	water	1 h	95	[57]
copper(I)@phosphorated SiO_2	water	1 h	94	[58]
Copper ferrite nanoparticles	water	6 h	87	[59]
CuI	PEG-400	16 h	83	[60]
$CuSO_4.5H_2O$/Sodiumascorbate	water	4h	92	[61]
GO@PTA-Cu	water	35 min	94	[62]
Cu@SBA-15@CF	water	2 h	90	[63]
CuO@mTiO_2@CF	water	6 h	89	[64]
98$BiFeO_3$-2RGO	water	5 h	91	[65]
$(Ag_{0.27}Ni_{0.73})_{37}RGO_{63}$	water	12 h	88	Present work

Spectral Data

Product of A3 coupling reaction (Table 2)

<u>Entry-1:</u> N,N-diethyl-3-phenylprop-2-yn-1-amine

^{1}H NMR ($CDCl_3$) δ= 7.45-7.43 (m, 2H), 7.32-7.30 (m, 3H), 3.66 (s, 2H), 2.67-2.62 (q, 4H), 1.15-1.12 (t, 6H) (Ref. [43])), IR (Liquid film cm^{-1}): ν =2974, 2815, 1600, 1494, 1380, 1318, 1195, 1089, 1054, 983, 754, 701, 613 [66]. LC-MS calculated.($C_{13}H_{17}N$) (M^+) :187.14 found : 188.00 [66].

<u>Entry-2</u>: N,N-diethyl-1,3-diphenylprop-2-yn-1-amine

^{1}H NMR ($CDCl_3$) δ= 7.54-7.38 (m, 10H), 1.70 (s,3H), 1.69 (m, 2H), 0.90 (m, 3H), 0.83 (m, 4H) (Ref. [43,66]), IR (Liquid film cm^{-1}): ν = 2983, 2806, 2306, 1990, 1931, 1852, 1615, 1547, 1485, 1370, 1197, 1067, 981, 750, 657 [66]. LC-MS calculated. (M^+) : 263.17 ($C_{19}H_{21}N$)found : 262.70 [66].

<u>Entry-3:</u> 1-(1,3-diphenylprop-2-yn-1-yl)piperidine

^{1}H NMR ($CDCl_3$) δ= 7.67-7.66 (m, 2H), 7.56-7.54 (m, 2H), 7.41-7.32 (m, 6H), 4.85(s,1H), 2.60 (m, 4H), 1.65-1.61 (m, 4H), 1.48-1.46 (m, 2H) (Ref. [43]), IR (Liquid film cm^{-1}): ν = 3286, 3062, 2935, 2779, 2723, 1694, 153, 1491, 1442, 1315, 1206, 1164, 1071, 999, 916, 829, 756, 684, 643. LC-MS calculated. (M^+) : 275.17 ($C_{20}H_{21}N$)found : 276.00.

<u>Entry-4</u>: 1-(3-phenyl-1-(p-tolyl)prop-2-yn-1-yl)piperidine

^{1}H NMR ($CDCl_3$) δ=7.54-7.52 (m,4H), 7.35-7.34 (m,3H), 7.20-7.18, (m, 2H), 4.80(s, 1H), 2.59 (s, 4H), 2.38 (s, 3H), 1.64-1.61 (m, 4H), 1.47-1.46 (m,2H) (Ref. [67]), IR (Liquid film cm^{-1}): ν =

3026, 2886, 2731, 1931, 1548, 1480, 1305, 1164, 1106, 984, 909, 815, 747, 689, 542. LC-MS calculated. (M^+) :289.18($C_{21}H_{23}N$) found : 290.00 .

<u>Entry-5</u>: 1-(1-(4-chlorophenyl)-3-phenylprop-2-yn-1-yl)piperidine

^{1}H NMR ($CDCl_3$) δ= 7.61-7.59 (m, 2H), 7.54-7.53 (m, 2H), 7.36-7.33 (m, 5H), 4.80 (s, 1H), 2.57 (s, 4H), 1.64-1.60 (m, 4H), 1.48-1.47 (m,2H) (Ref. [42]), IR (Liquid film cm^{-1}): ν = 3285, 3057, 2840, 2716, 1924, 1699, 1574, 1481, 1378, 1285, 1202, 1089, 1006, 820, 748, 686, 549. LC-MS calculated. (M^+) : 309.83($C_{20}H_{20}NCl$) found : 310.00 [42].

<u>Entry-6</u>: 1-(1-(4-bromophenyl)-3-phenylprop-2-yn-1-yl)piperidine

^{1}H NMR ($CDCl_3$) δ= 7.78-7.70 (m,2H), 7.56-7.48 (m, 4H) 7.36-7.35 (m, 3H), 4.79 (s, 1H) 2.57 (s, 4H), 1.63-1.59 (m, 4H) , 1.48-1.46 (m, 2H)), IR (Liquid film cm^{-1}): ν = 2932, 2850, 2798, 1671, 1599, 1485, 1444, 1392, 1320, 1279, 1165, 1072, 1000, 814, 752, 690, 534. LC-MS calculated. (M^+) : 354.28 ($C_{20}H_{20}NBr$) found : 355.80 [42].

<u>Entry-7</u>: 1-(3-phenylprop-2-yn-1-yl)piperidine

^{1}H NMR ($CDCl_3$) δ= 7.46-7.45 (m, 2H), 7.32-7.30 (m, 3H), 3.50 (s, 2H), 2.59 (s, 4H), 1.69-1.65 (m,4H), 1.47 (s, 2H) (Ref. [43]), IR (Liquid film cm^{-1}): ν = 3286, 3062, 2935, 2799, 2723, 1694, 1593, 1491, 1442, 1315, 1206, 1164, 1071, 999, 916, 829, 756, 684, 643 [66]. LC-MS calculated. (M^+) :199.29($C_{14}H_{17}N$) found : 199.70 [66].

<u>Entry-8</u>: N-(1,3-diphenylprop-2-yn-1-yl)aniline

^{1}H NMR ($CDCl_3$) δ= 8.56 (d, 2H), 8.31(d, 2H), 8.09-8.07 (m, 2H), 7.45 (m,2H), 7.28 (m, 3H), (Ref. [43,45]), IR (Liquid film cm^{-1}): ν = 3060, 2915, 2853, 1619, 1441, 1361, 1309, 1175, 1071, 978, 906, 761, 689, 538. LC-MS calculated. (M^+) :283.37($C_{21}H_{17}N$) found : 284.00 [45]

<u>Entry-9</u>: N-(3-phenyl-1-(p-tolyl)prop-2-yn-1-yl)aniline

^{1}H NMR ($CDCl_3$) δ= 8.46 (m,1H), 7.86-7.84 (m, 3H), 7.44 (m, 3H), 7.27 (m,6H), 2.46 (m, 4H) (Ref. [43,45]), IR (Liquid film cm^{-1}): ν = 3060, 2915, 2853, 1619, 1441, 1361, 1309, 1175, 1071, 978, 906, 761, 689, 538. LC-MS calculated. (M^+) :297.39($C_{22}H_{19}N$) found : 298.00 [45].

<u>Entry-10</u>: N-(1-(4-methoxyphenyl)-3-phenylprop-2-yn-1-yl)aniline

^{1}H NMR ($CDCl_3$) δ= 8.50 (s, 1H), 7.96-7.94 (m, 2H), 7.53 (m, 3H), 7.52-7.43 (m,2H), 7.28 (m, 3H) (Ref. [43,45]), IR (Liquid film cm^{-1}): ν = 3530, 3012, 2835, 1694, 1593, 1500, 1305, 1246, 1163, 1101, 1029, 967, 895, 822, 758, 693, 542. LC-MS calculated. ($C_{22}H_{19}NO$) (M^+) : 313.39 found : 314.00 [45]

<u>Entry-11</u>: N-(1-(4-nitrophenyl)-3-phenylprop-2-yn-1-yl)aniline

^{1}H NMR ($CDCl_3$) δ= 8.41 (s, 1H) 7.90-7.88 (m, 3H), 7.42 (m, 2H), 7.25-7.23(m, 4H), 7.03-7.00 (m,3H), 3.90-3.89 (m, 4H) (Ref. [43,45]), IR (Liquid film cm^{-1}): ν = 3060, 2299, 1513, 1341, 1182, 920, 848, 765, 693. LC-MS calculated. ($C_{21}H_{16}N_2O_2$) (M^+): 328.36 found: 329.00 [45].

Product of 'Click reaction'

2-phenyl-2-(4-phenyl-1*H*-1,2,3-triazole-1-yl)ethanol

Solid, m.p. 126-128°C (reported 125-127 °C (Ref.[62])). IR (KBr): 3427, 3123, 3089, 3029, 2939, 1493, 1455, 1431, 1223, 1084, 1057, 755, 693 cm^{-1}. LC-MS (EI) m/z calculated for $C_{16}H_{15}N_3O$ 265.12, observed 266.00 (reported 265.12 (Ref. [62])).

2-(4-Phenyl-1*H*-1,2,3-triazol-1-yl)cyclohexanol

Solid, m.p. 170-172 °C (reported 167.8-171.8 °C (Ref.[62])). IR (KBr): 3298, 3119, 2938, 2858, 1447, 1232, 1054, 763, 696 cm^{-1} LC-MS (EI) m/z calculated for C_{14} $H_{17}N_3O$ 243.13, observed 244.00 (HRMS reported for $C_{14}H_{18}N_3O$ 244.14 (Ref. [62]).

1,3-Bis(4-phenyl-1H-1,2,3-triazol-1-yl)propan-2-ol

Solid, m.p. 235-237 °C (reported 233-236°C (Ref. [62])), IR (KBr): 2959, 2938, 2858, 1447, 1232, 1054,763 cm^{-1}. LC-MS (EI) m/z calculated for C_{19} $H_{19}N_6O$ 346.13, observed 347.00 (HRMS reported for $C_{19}H_{19}N_6O$ 346.20 (Ref. [62]).

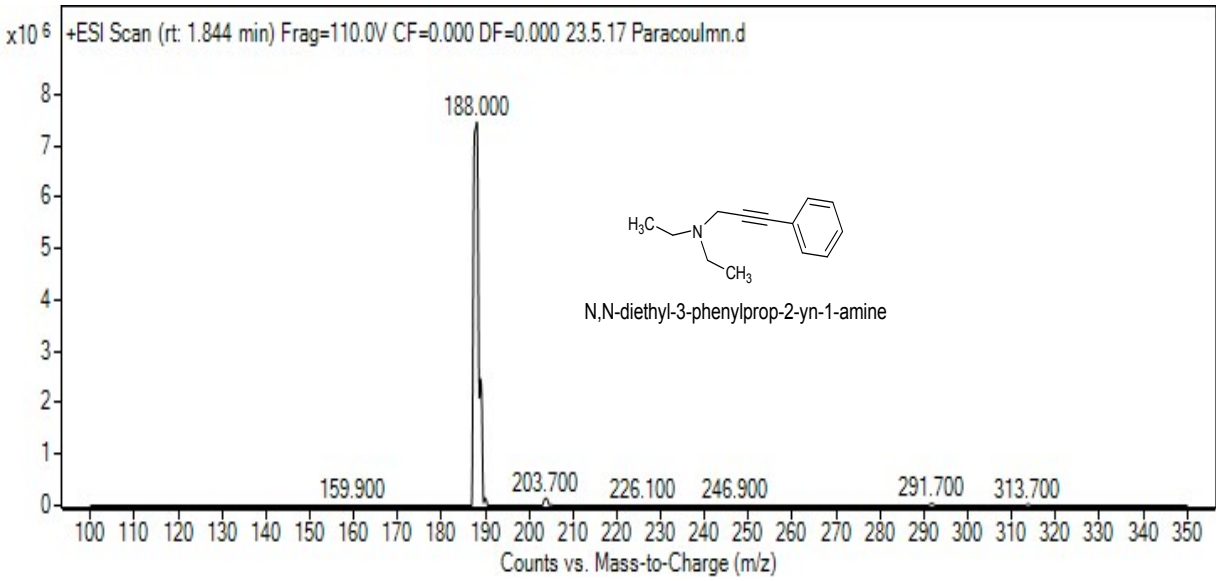

Fig. S25a. LC-MS full scan of N,N-diethyl-3-phenylprop-2-yn-1-amine.

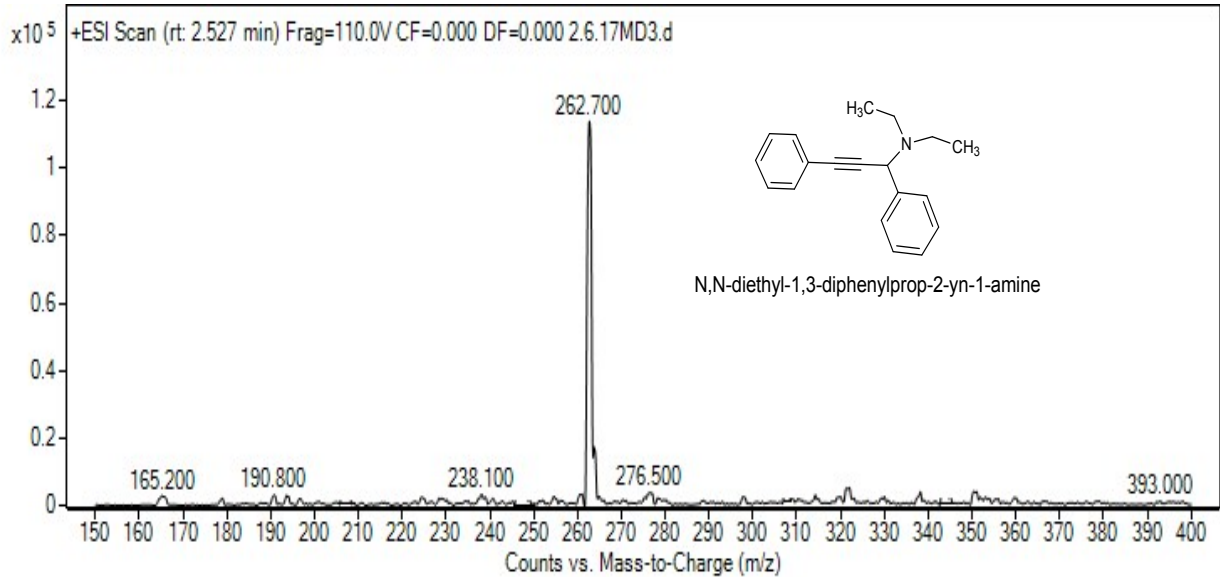

Fig. S25b. LC-MS full scan of N,N-diethyl-1,3-diphenylprop-2-yn-1-amine.

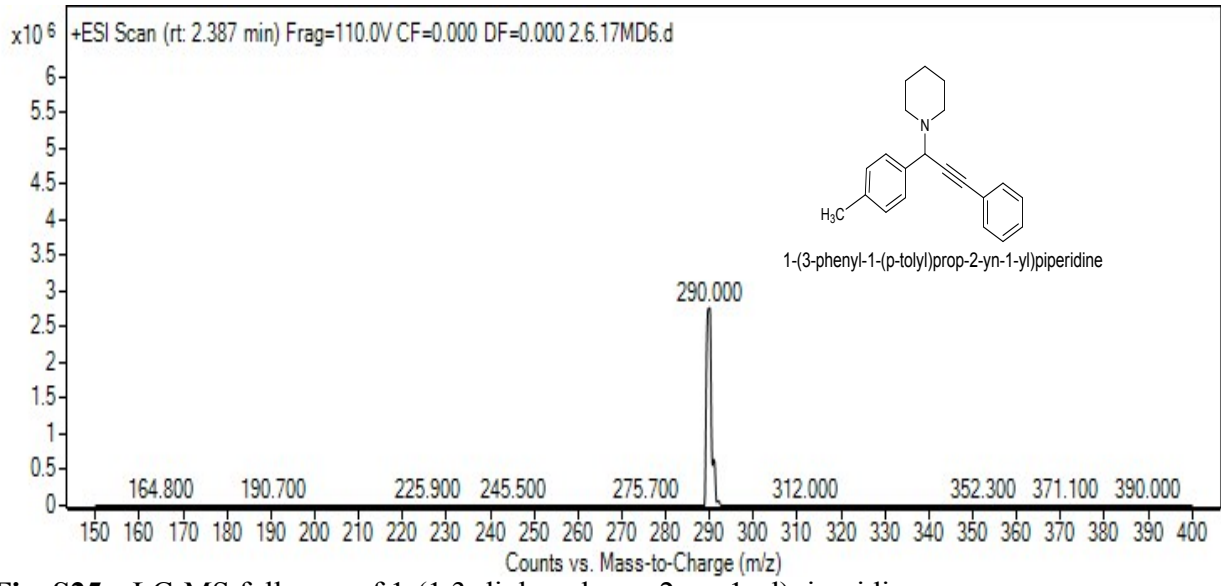

Fig. S25c. LC-MS full scan of 1-(1,3-diphenylprop-2-yn-1-yl)piperidine.

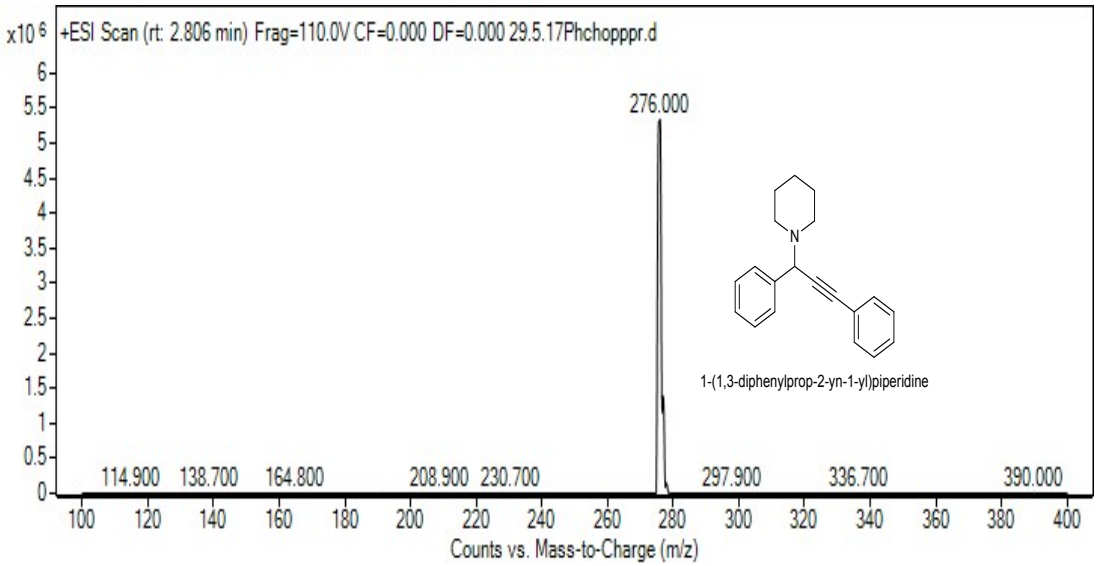

Fig. S25d. LC-MS full scan of 1-(3-phenyl-1-(p-tolyl)prop-2-yn-1-yl)piperidine.

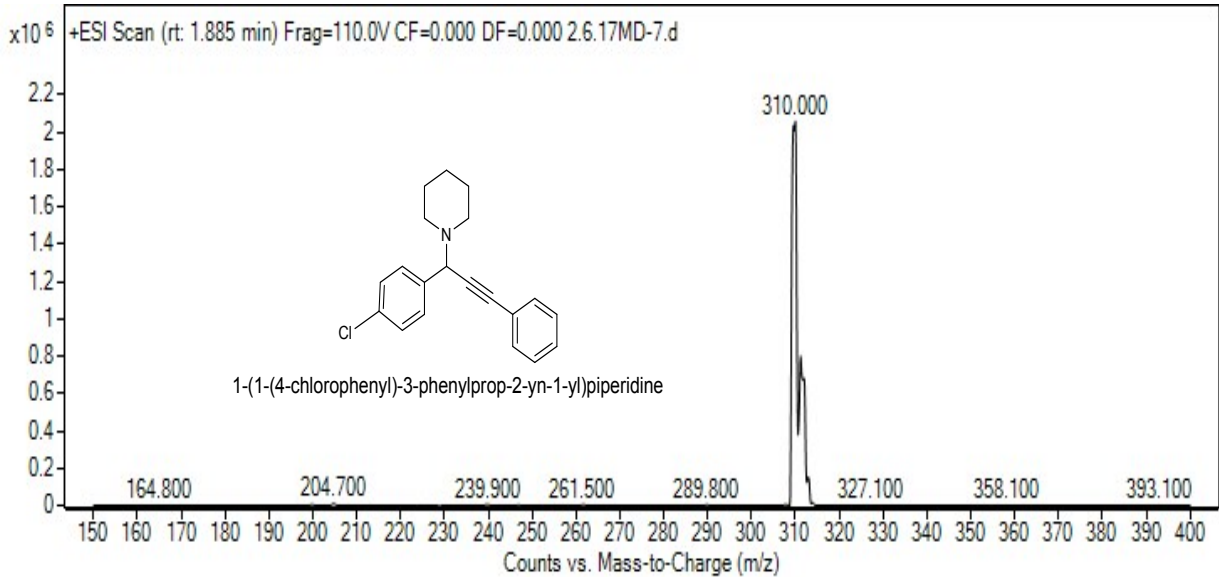

Fig. S25e. LC-MS full scan of 1-(1-(4-chlorophenyl)-3-phenylprop-2-yn-1-yl)piperidine

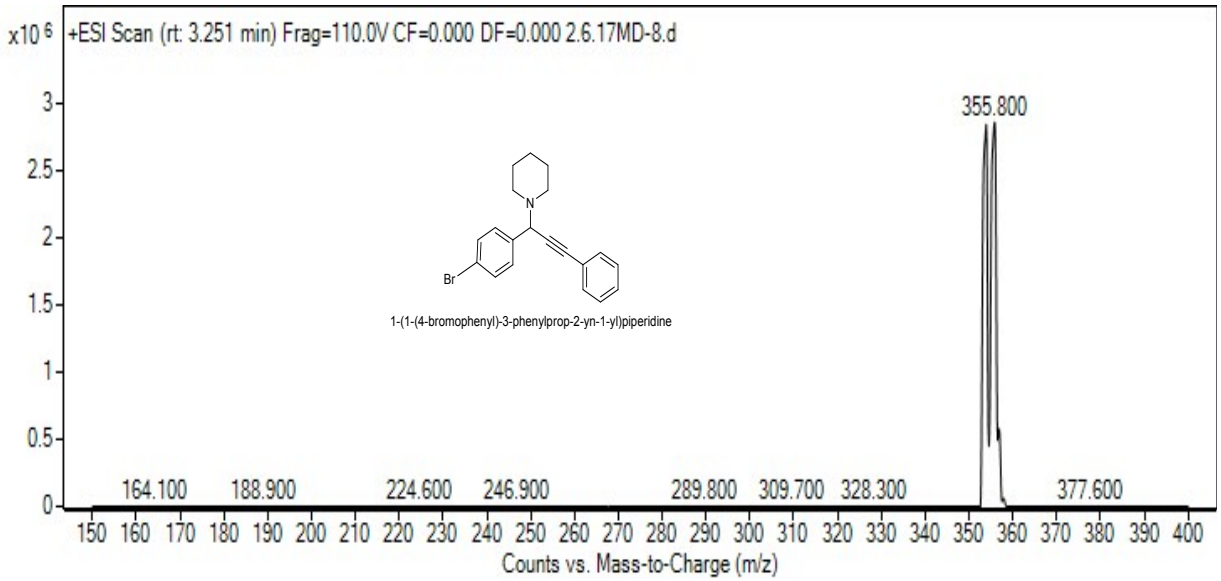

Fig. S25f. LC-MS full scan of 1-(1-(4-bromophenyl)-3-phenylprop-2-yn-1-yl)piperidine.

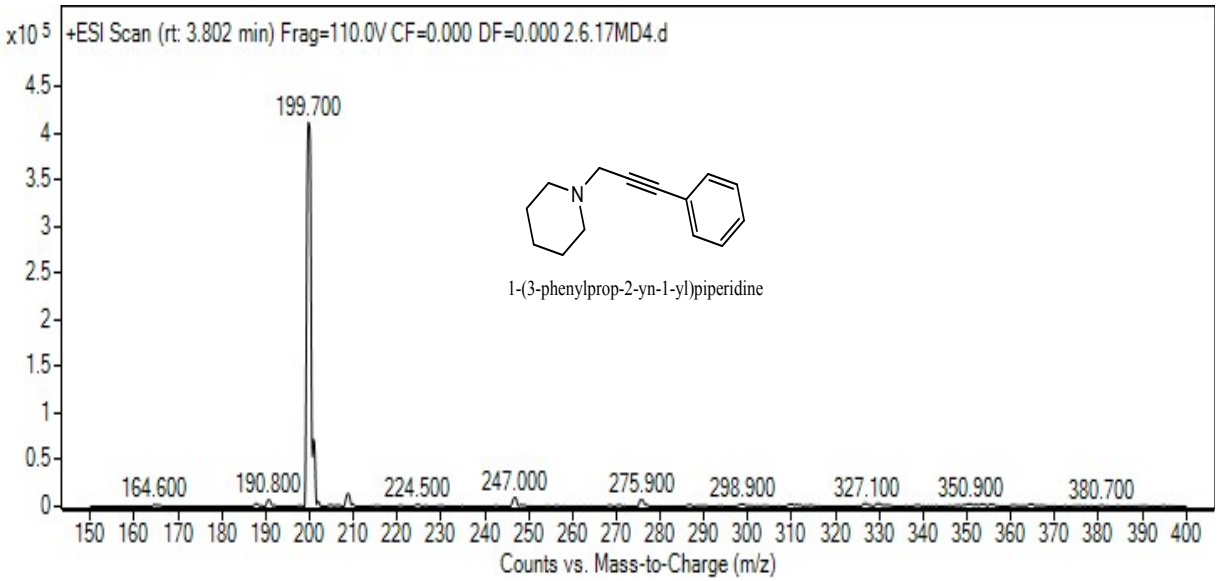

Fig. S25g. LC-MS full scan of 1-(3-phenylprop-2-yn-1-yl)piperidine.

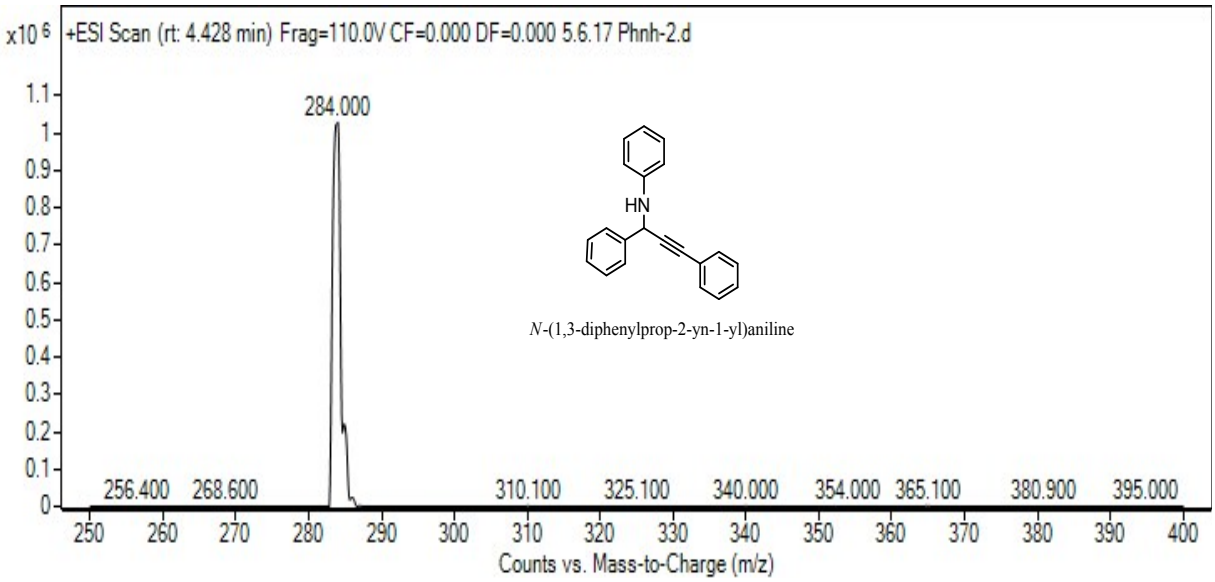

Fig. S25h. LC-MS full scan of N-(1,3-diphenylprop-2-yn-1-yl)aniline.

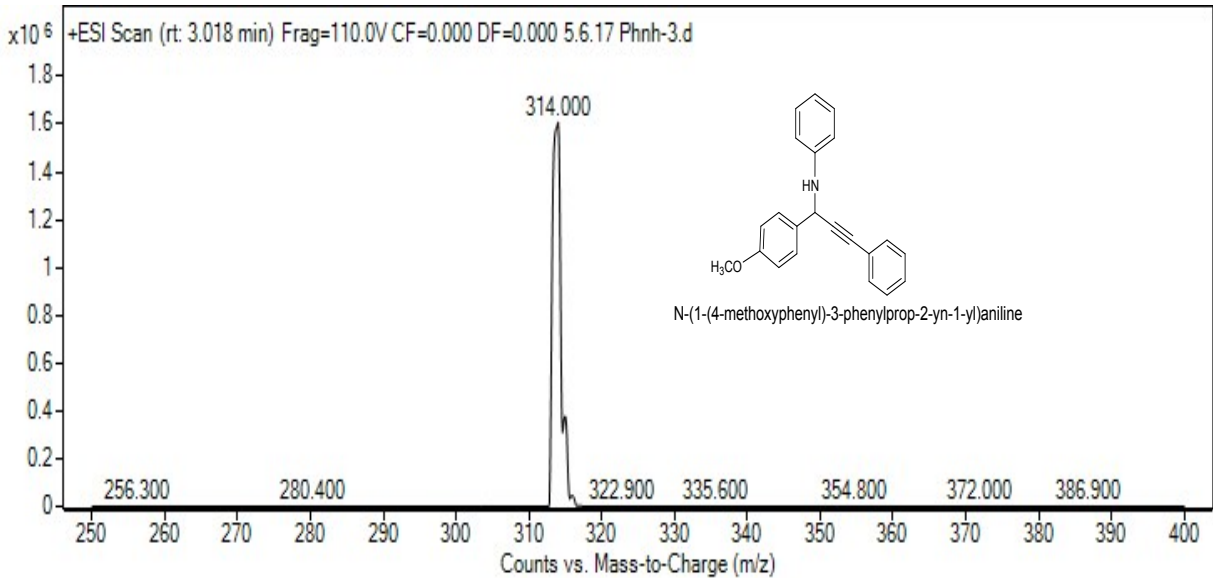

Fig. S25i. LC-MS full scan of N-(3-phenyl-1-(p-tolyl)prop-2-yn-1-yl)aniline.

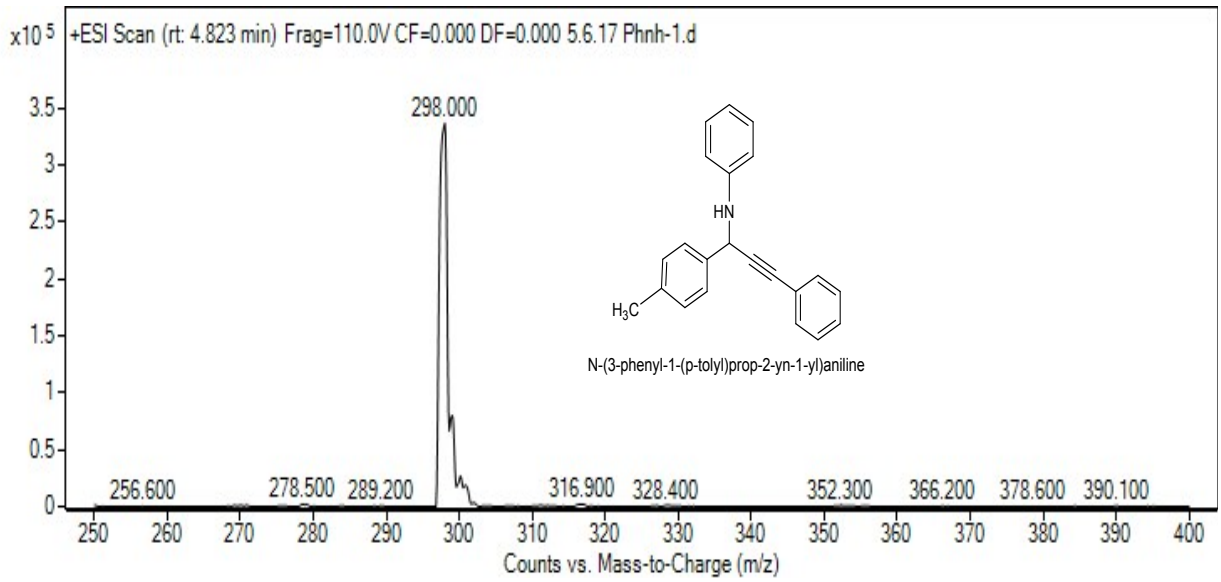

Fig. S25j. LC-MS full scan of N-(1-(4-methoxyphenyl)-3-phenylprop-2-yn-1-yl)aniline.

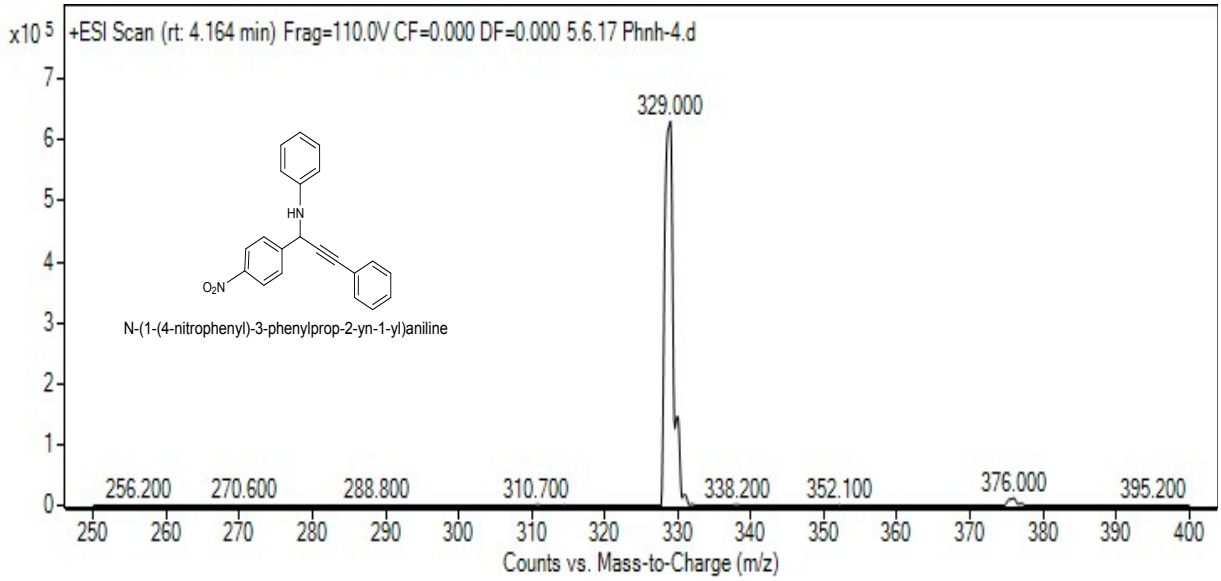

Fig. S25k. LC-MS full scan of N-(1-(4-nitrophenyl)-3-phenylprop-2-yn-1-yl)aniline.

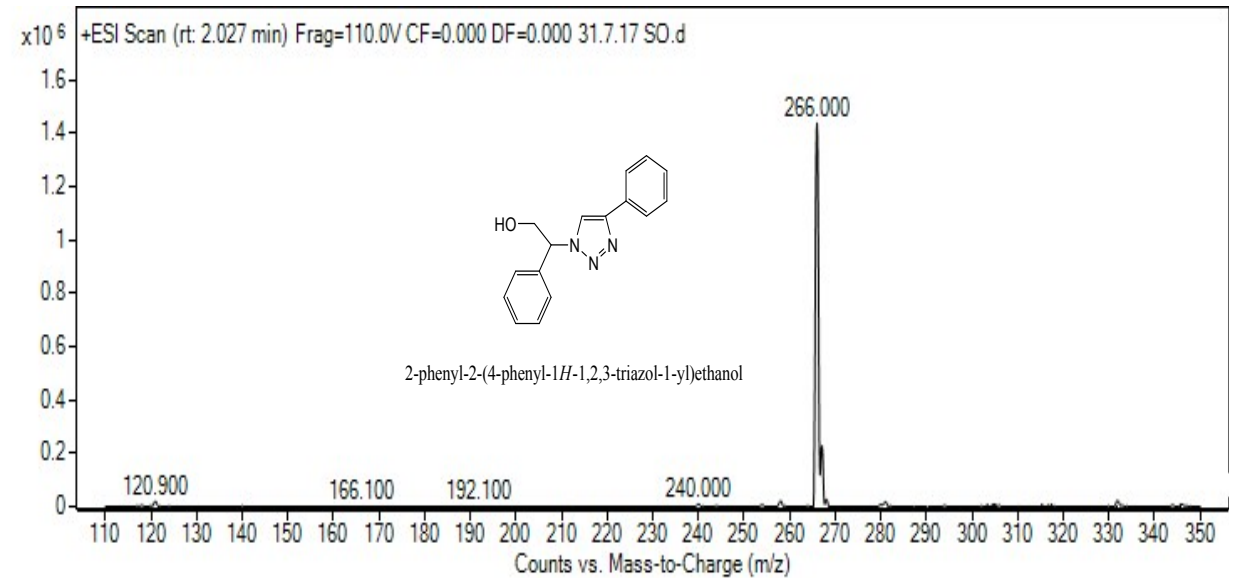

Fig. S25l. LC-MS full scan of 2-phenyl-2-(4-phenyl-1H-1,2,3-triazole-1-yl)ethanol.

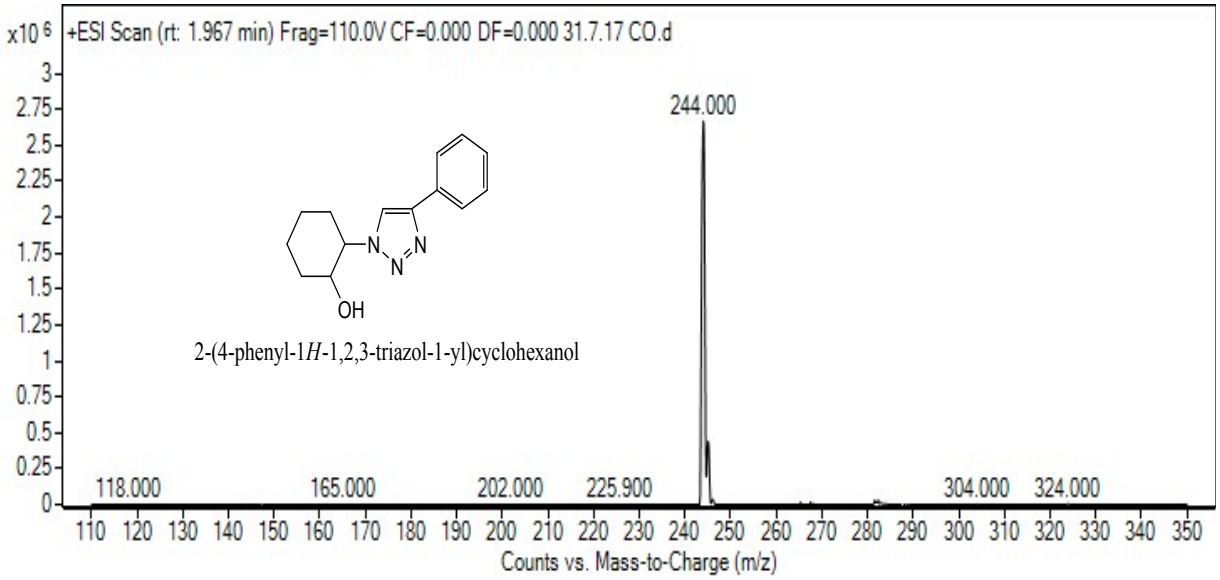

Fig. S25m. LC-MS full scan of 2-(4-phenyl)-1H-1,2,3-triazole-1-yl)cyclohexanol.

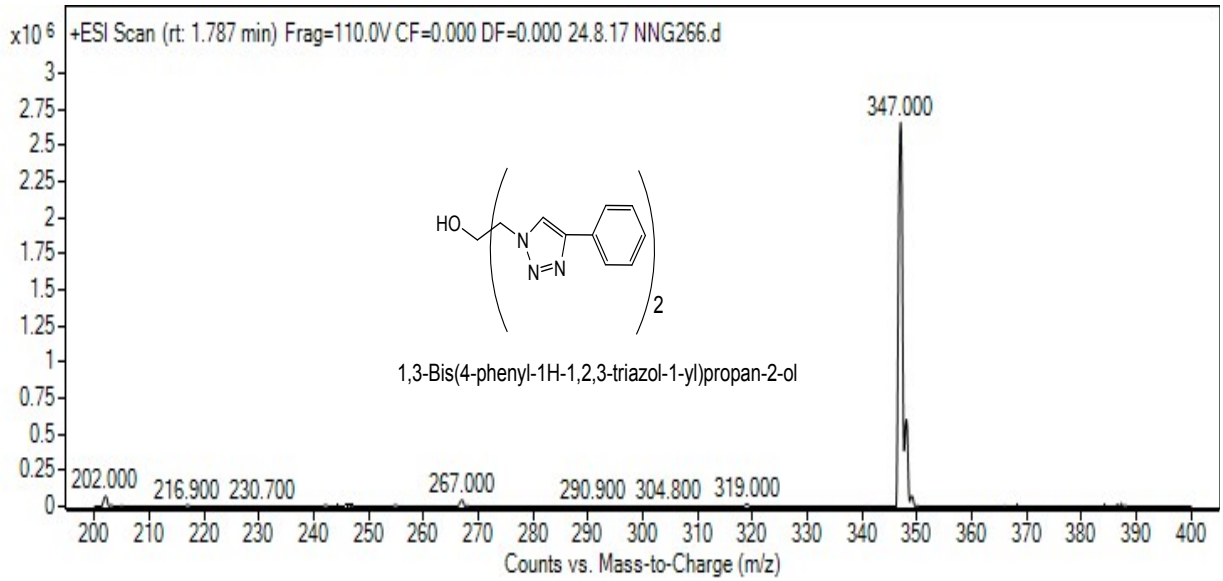

Fig. S25n. LC-MS full scan of 1,3-Bis(4-phenyl-1H-1,2,3-triazole-1-yl)propan-2-ol.

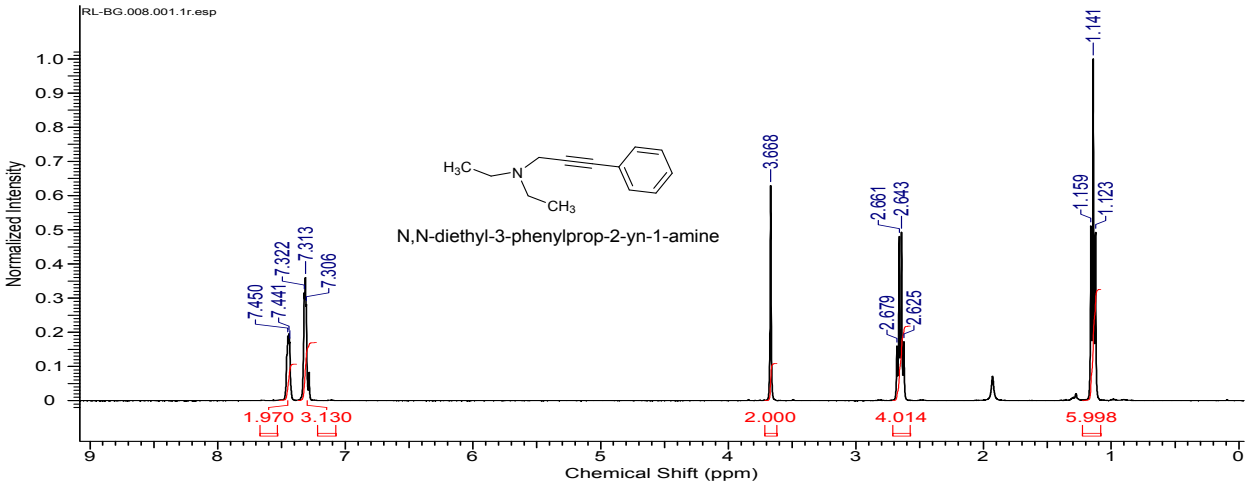

Fig. S26a. ^{1}H NMR spectrum of N,N-diethyl-3-phenylprop-2-yn-1-amine synthesized via A3 coupling reaction.

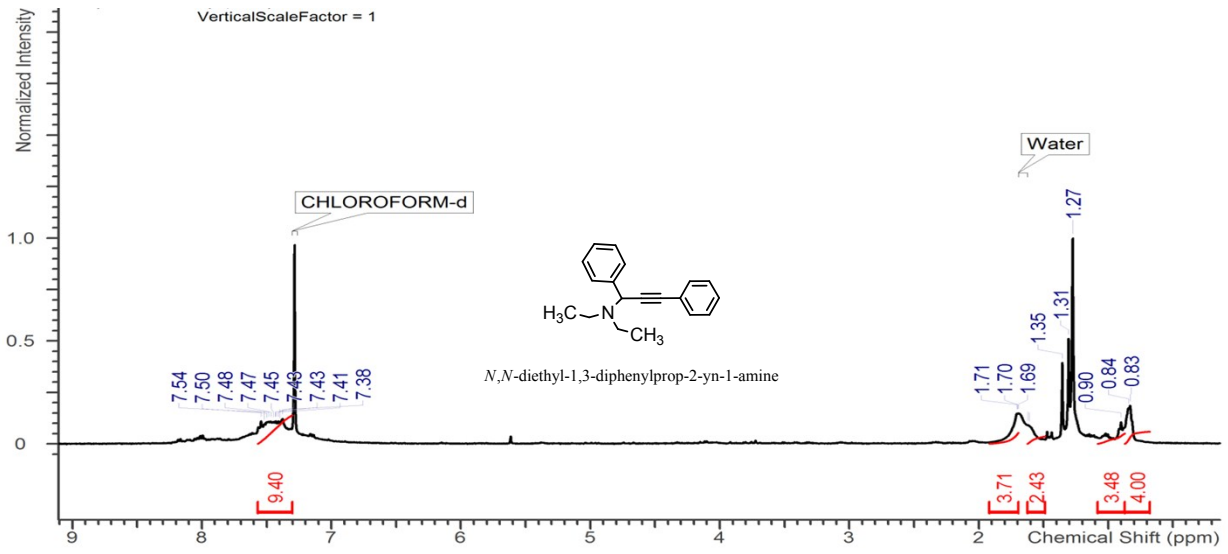

Fig. S26b. ^{1}H NMR spectrum of N,N-diethyl-1,3-diphenylprop-2-yn-1-amine synthesized via A3 coupling reaction.

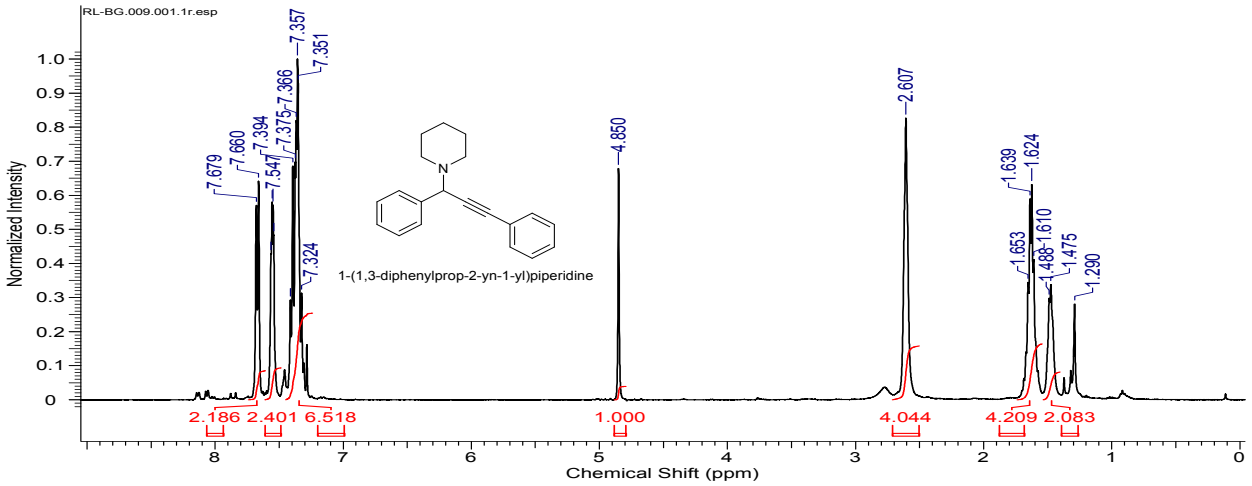

Fig. S26c. ^{1}H NMR spectrum of 1-(1,3-diphenylprop-2-yn-1-yl)piperidine synthesized via A3 coupling reaction.

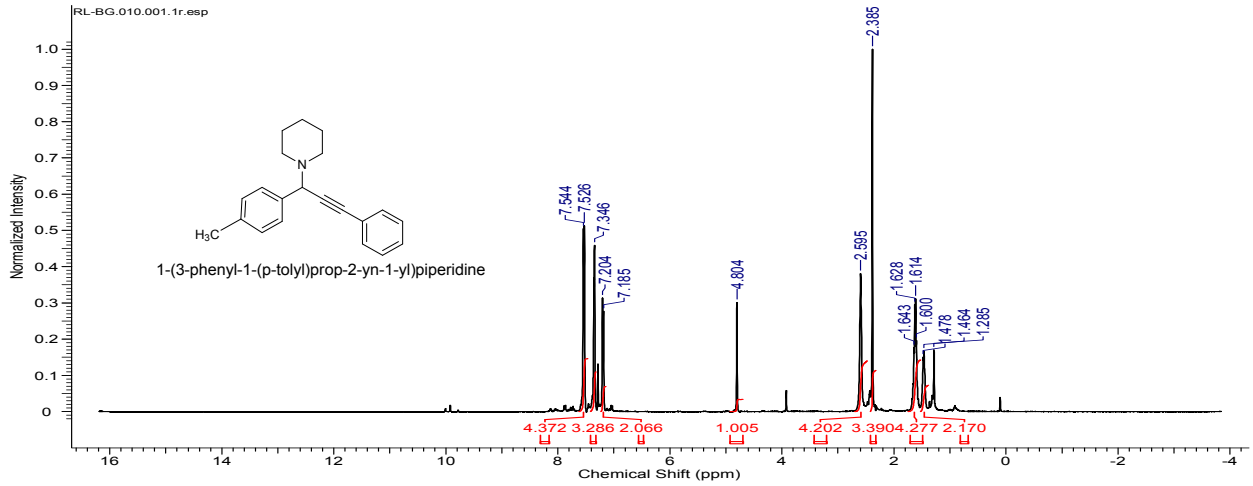

Fig. S26d. ^{1}H NMR spectrum of 1-(3-phenyl-1-(p-tolyl)prop-2-yn-1-yl)piperidine synthesized via A3 coupling reaction.

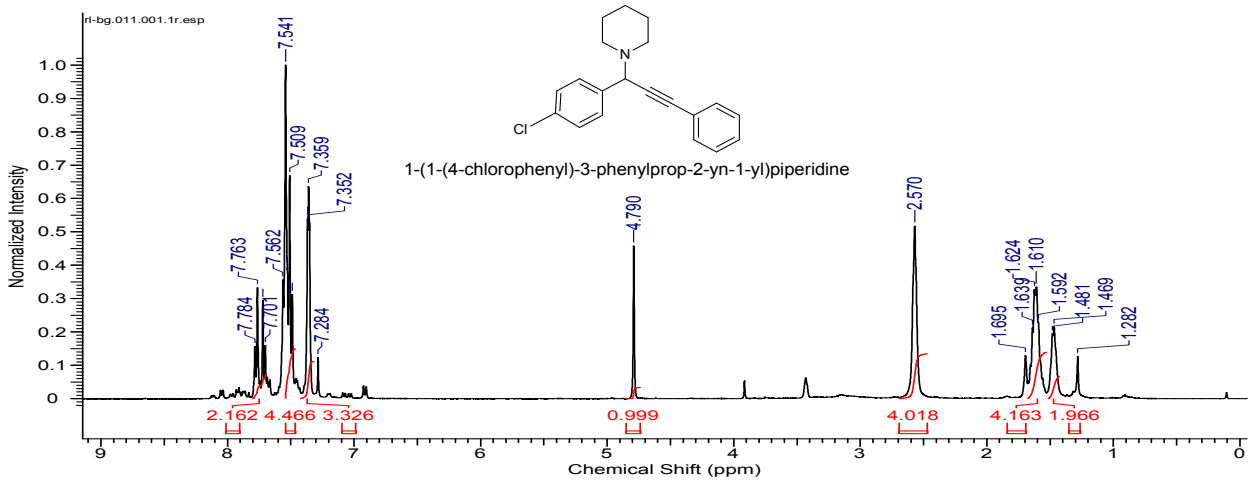

Fig. S26e. ^{1}H NMR spectrum of 1-(1-(4-chlorophenyl)-3-phenylprop-2-yn-1-yl)piperidine synthesized via A3 coupling reaction.

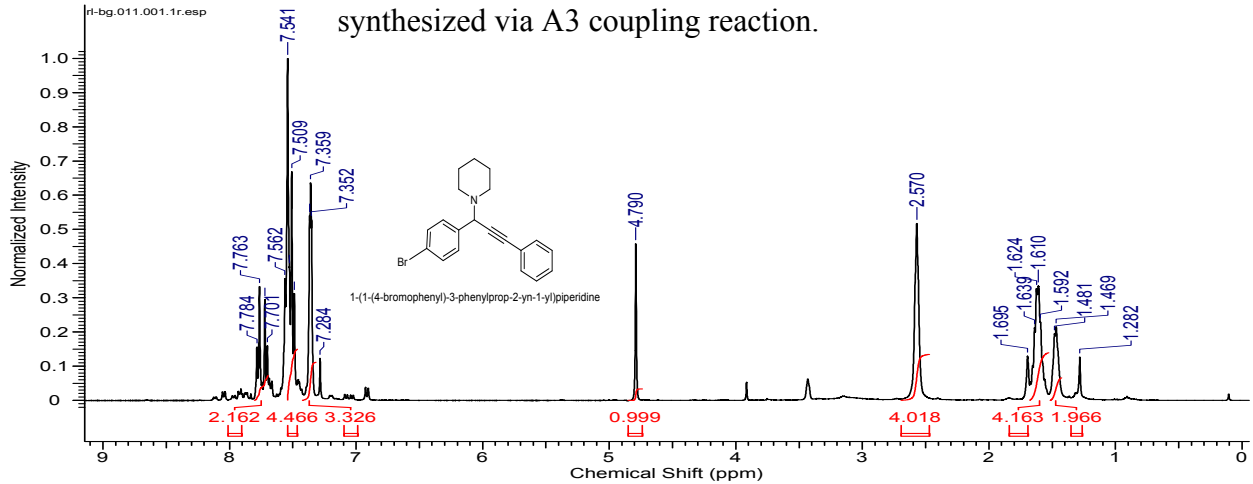

Fig. S26f. ^{1}H NMR spectrum of 1-(1-(4-bromophenyl)-3-phenylprop-2-yn-1-yl)piperidine synthesized via A3 coupling reaction.

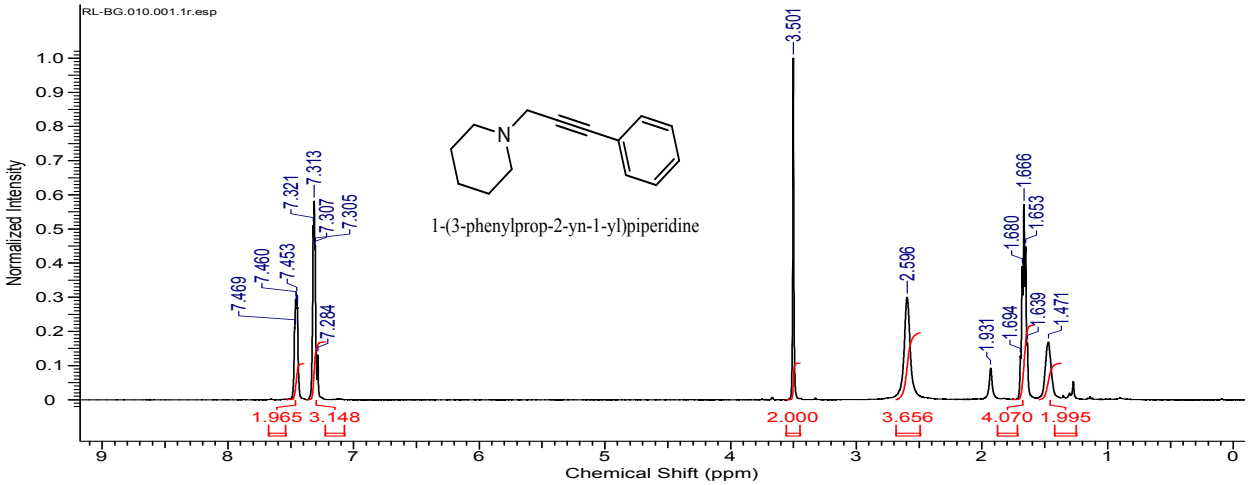

Fig. S26g. ^{1}H NMR spectrum of 1-(3-phenylprop-2-yn-1-yl)piperidine synthesized via A3 coupling reaction.

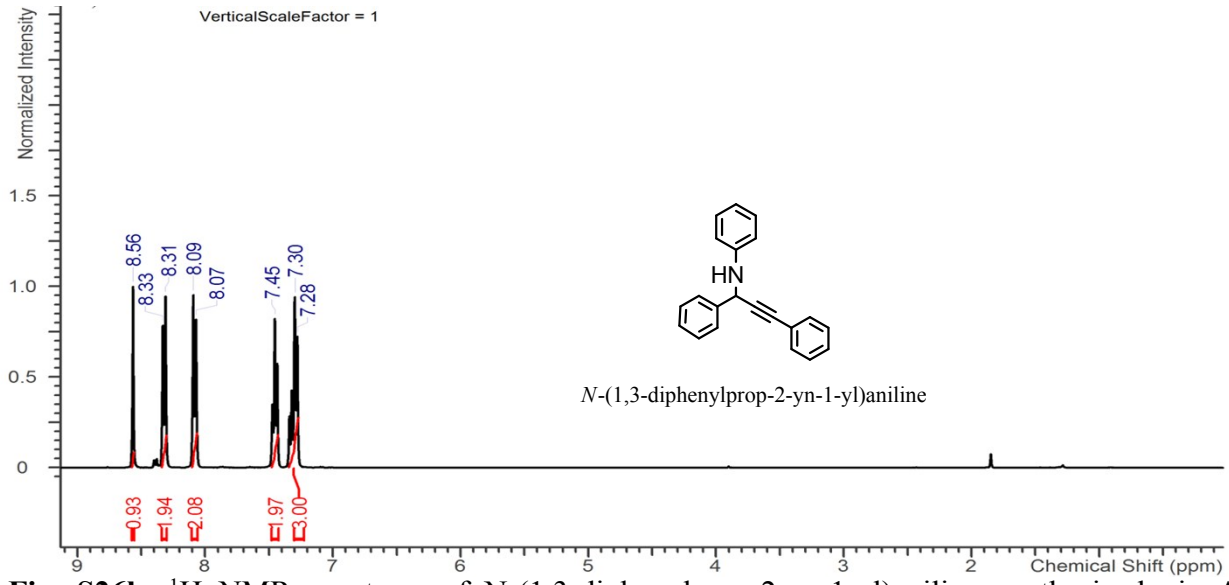

Fig. S26h. ^{1}H NMR spectrum of N-(1,3-diphenylprop-2-yn-1-yl)aniline synthesized via A3 coupling reaction.

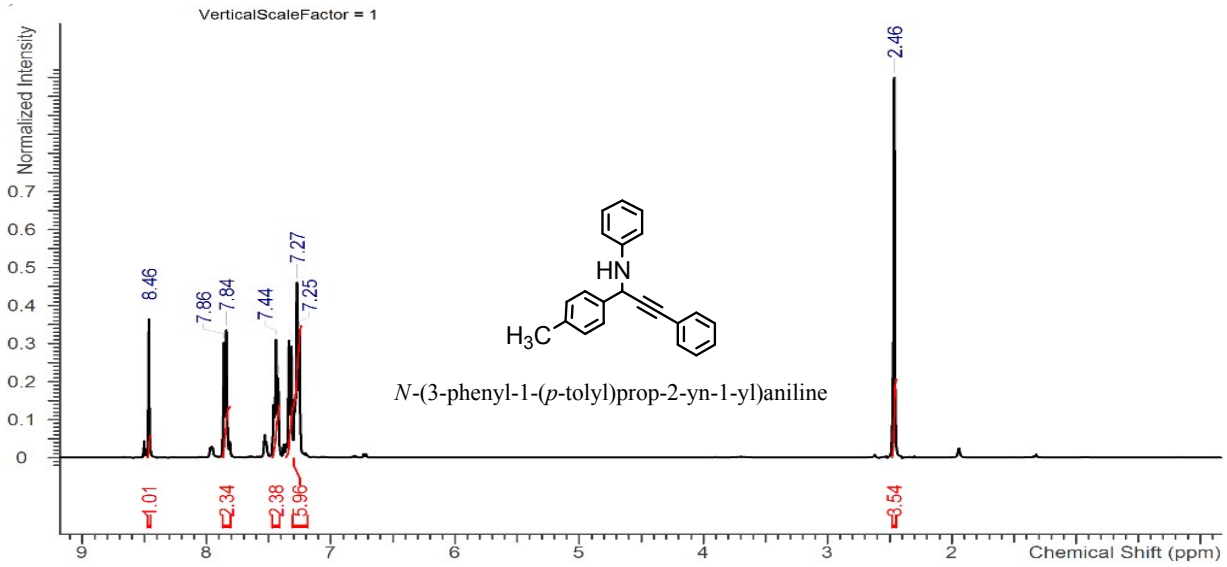

Fig. S26i. ^{1}H NMR spectrum of N-(3-phenyl-1-(p-tolyl)prop-2-yn-1-yl)aniline synthesized via A3 coupling reaction.

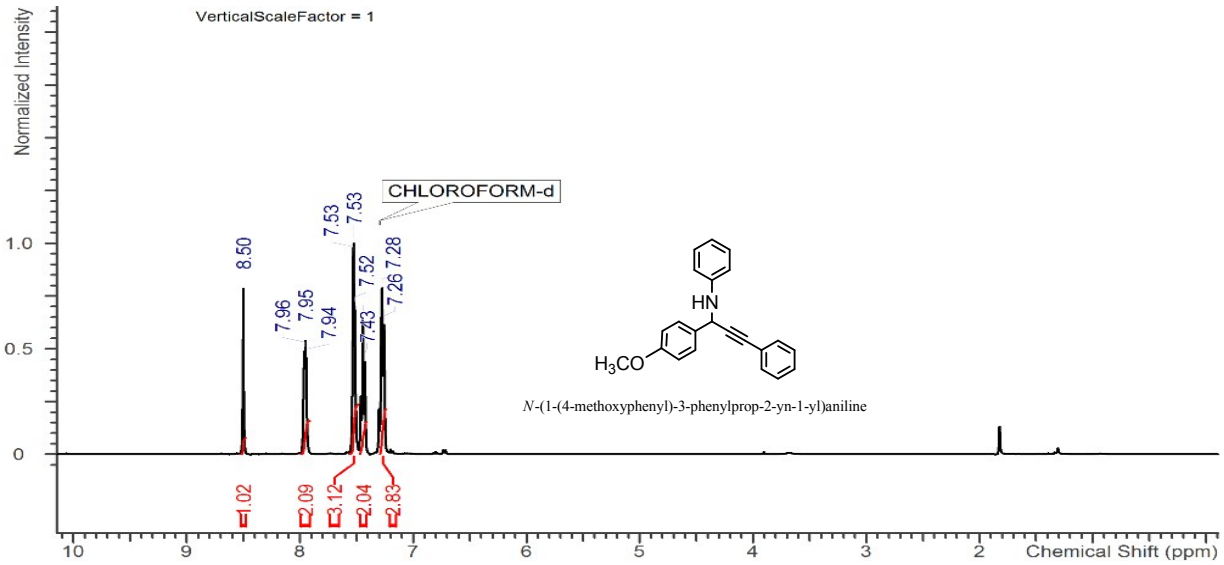

Fig. S26j. ^{1}H NMR spectrum of 1-(3-phenylprop-2-yn-1-yl)aniline synthesized via A3 coupling reaction.

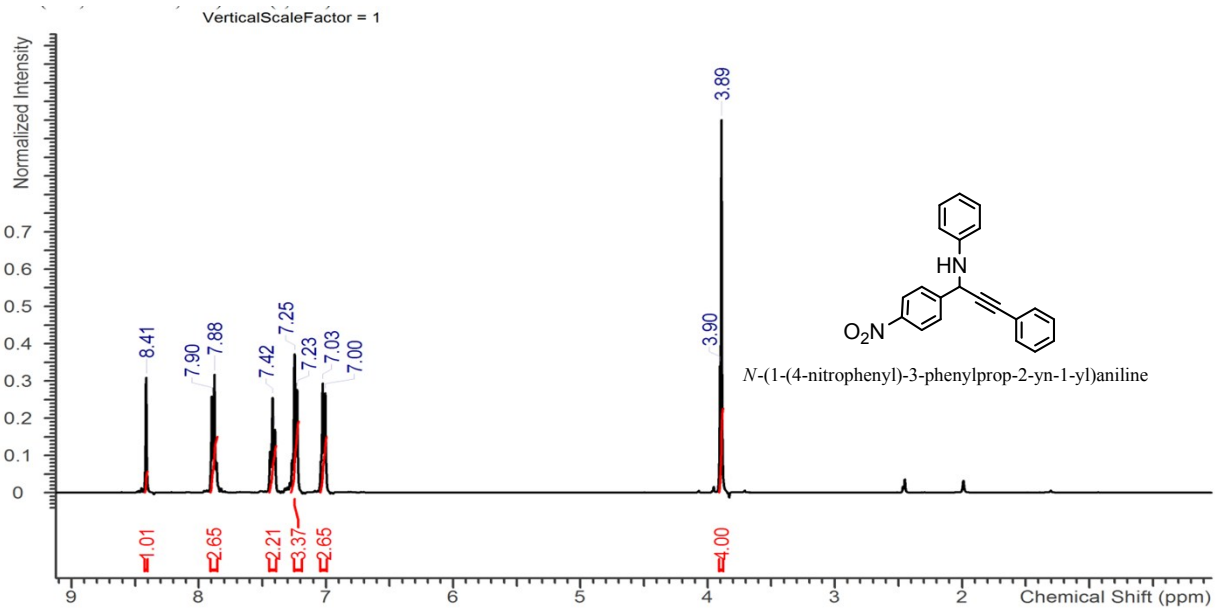

Fig. S26k. ^{1}H NMR spectrum of N-(1-(4-nitrophenyl)-3-phenylprop-2-yn-1-yl)aniline synthesized via A3 coupling reaction.

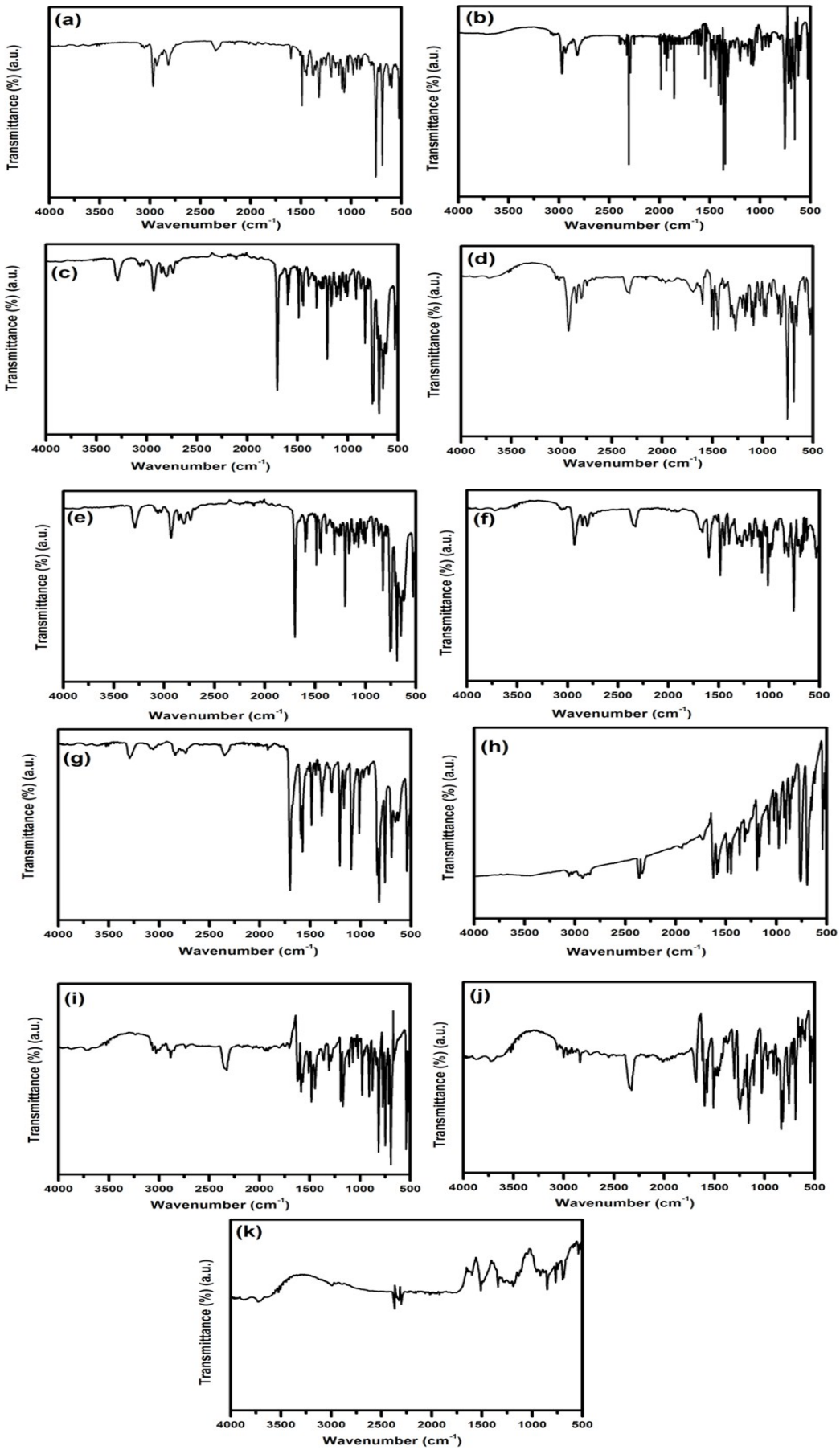
(a)
(b)
(c)
(d)
(e)
(f)
(g)
(h)
(i)
(j)
(k)
Transmittance (%) (a.u.)
Wavenumber (cm^{-1})
4000 3500 3000 2500 2000 1500 1000 500

Fig. S27. FT-IR spectrum of (a) N,N-diethyl-3-phenylprop-2-yn-1-amine, (b) N,N-diethyl-1,3-diphenylprop-2-yn-1-amine, (c) 1-(1,3-diphenylprop-2-yn-1-yl)piperidine, (d) 1-(3-phenyl-1-(p-tolyl)prop-2-yn-1-yl)piperidine, (e) 1-(1-(4-chlorophenyl)-3-phenylprop-2-yn-1-yl)piperidine, (f) 1-(1-(4-bromophenyl)-3-phenylprop-2-yn-1-yl)piperidine, (g) 1-(3-phenylprop-2-yn-1-yl)piperidine, (h) N-(1,3-diphenylprop-2-yn-1-yl)aniline, (i) N-(3-phenyl-1-(p-tolyl)prop-2-yn-1-yl)aniline, (j) N-(1-(4-methoxyphenyl)-3-phenylprop-2-yn-1-yl)aniline, (k) N-(1-(4-nitrophenyl)-3-phenylprop-2-yn-1-yl)aniline.

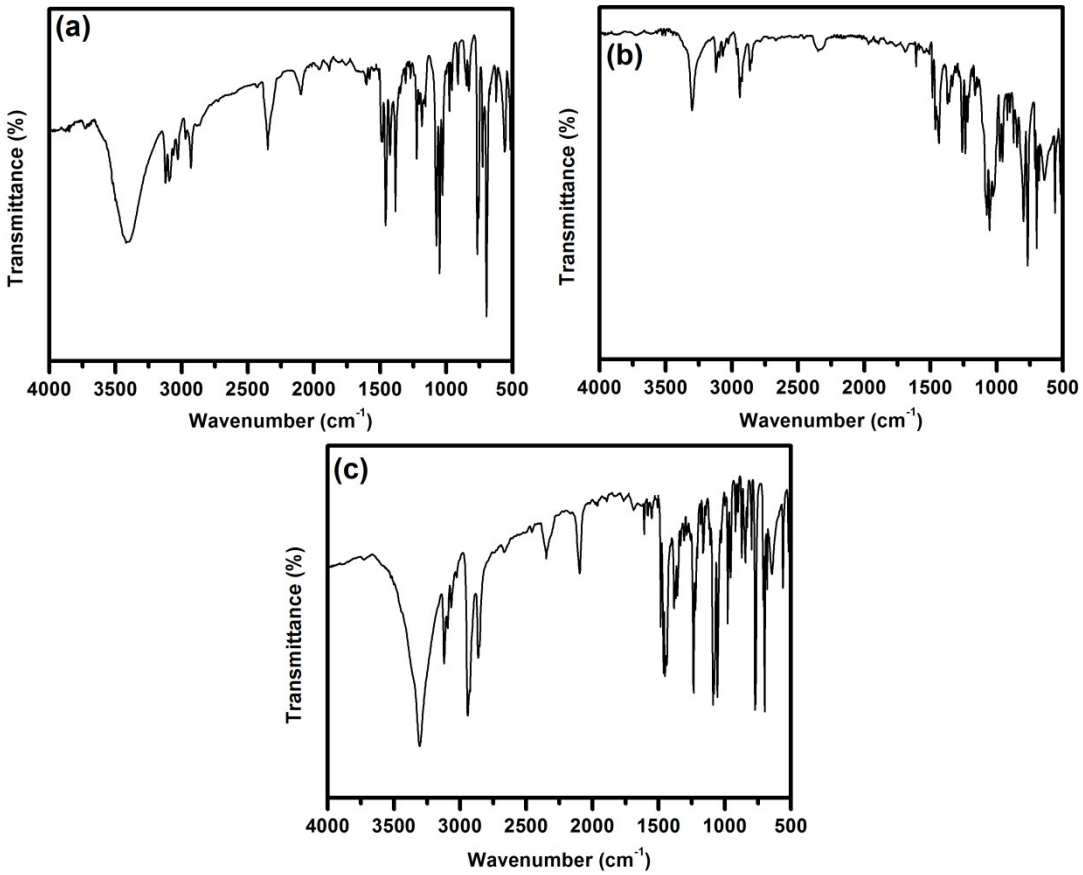

Fig. S28. FT-IR spectrum of (a) 2-phenyl-2-(4-phenyl-1*H*-1,2,3-triazole-1-yl) ethanol (b) 2-(4-Phenyl-1*H*-1,2,3-triazol-1-yl) cyclohexanol (c) 1,3-Bis(4-phenyl-1H-1,2,3-triazol-1-yl)propan-2-ol.

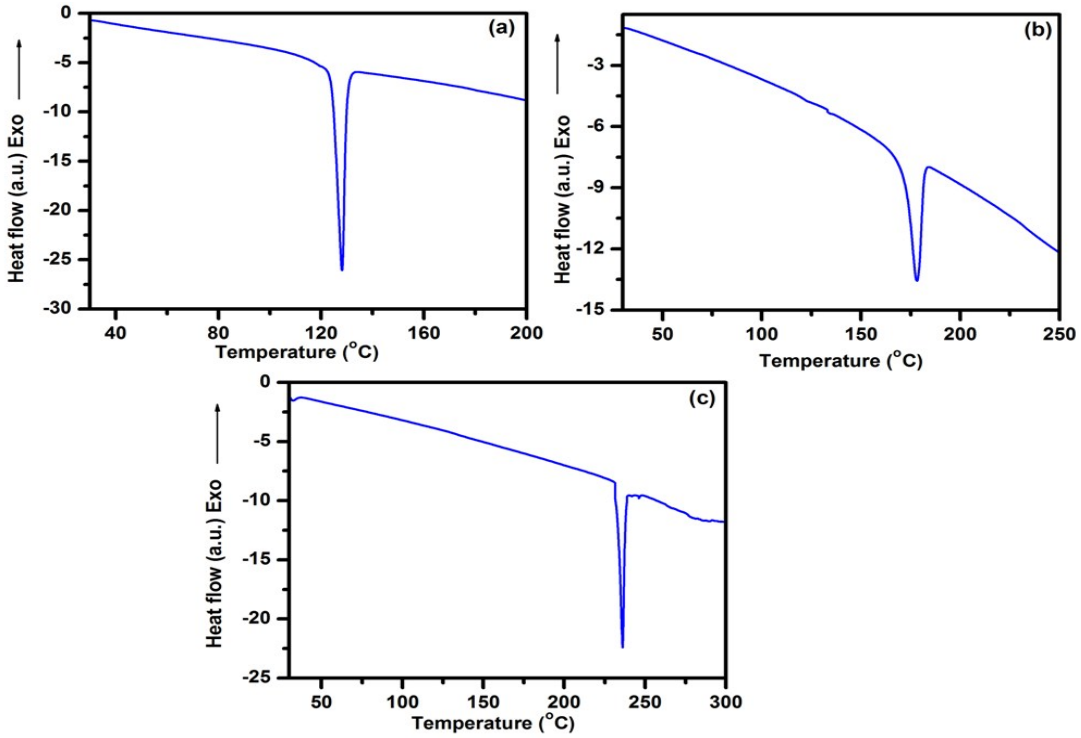

Fig. S29. DSC of (a) 2-phenyl-2-(4-phenyl-1*H*-1,2,3-triazole-1-yl) ethanol and (b) 2-(4-Phenyl-1*H*-1,2,3-triazol-1-yl)cyclohexanol (c) 1,3-Bis(4-phenyl-1H-1,2,3-triazol-1-yl)propan-2-ol.

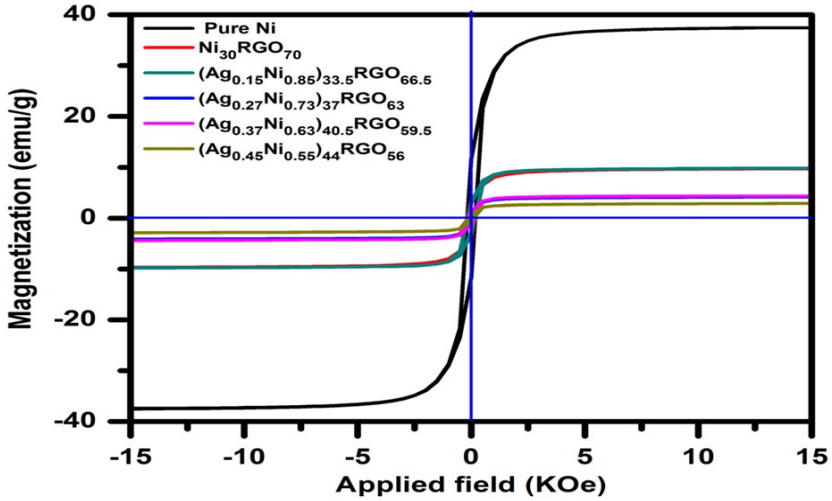

Fig. S30. Room temperature magnetic hysteresis loop of Pure Ni, $Ni_{30}RGO_{70}$, $(Ag_{0.15}Ni_{0.85})_{33.5}RGO_{66.5}$, $(Ag_{0.27}Ni_{0.73})_{37}RGO_{63}$, $(Ag_{0.37}Ni_{0.63})_{40.5}RGO_{59.5}$, and $(Ag_{0.45}Ni_{0.55})_{44}RGO_{56}$.

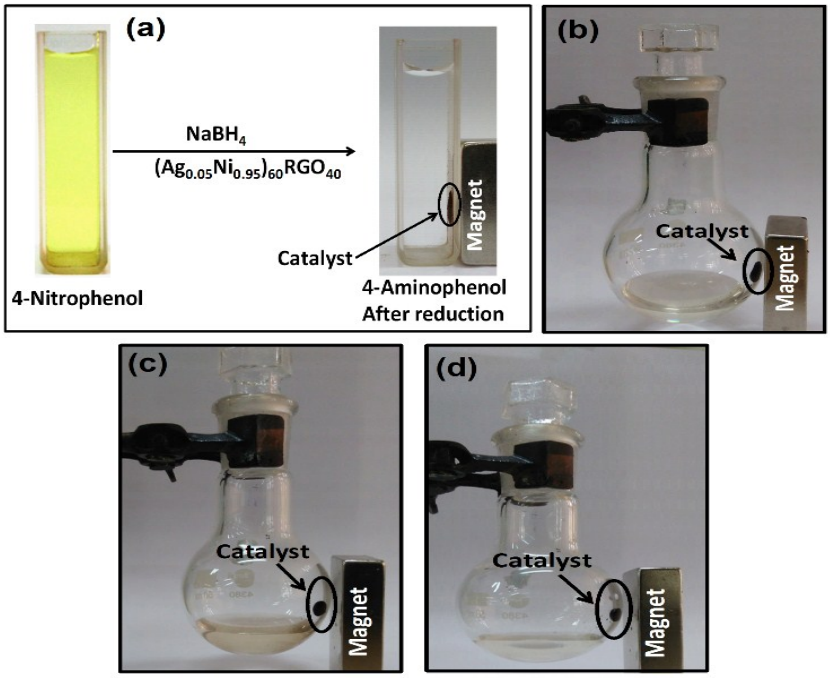

Fig. S31. Magnetic separation of the catalyst by applying a magnet externally after completion of (a) reduction of 4-NP in presence of $NaBH_4$, (b) A3 coupling reaction, (c) epoxidation of styrene, and (d) Click reaction.

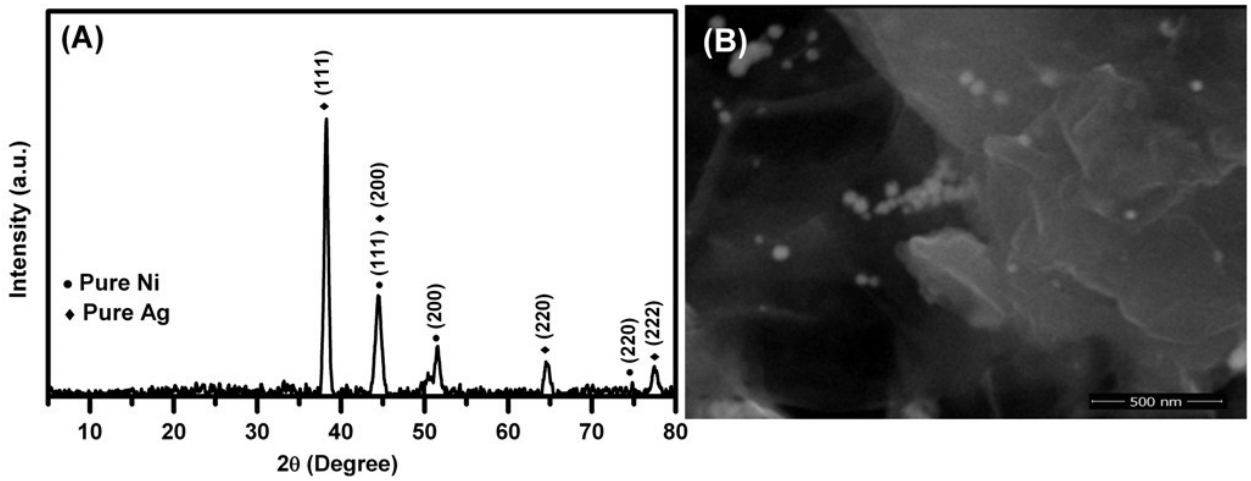

Fig. S32. (A) XRD and (B) FESEM image of the recycled $(Ag_{0.27}Ni_{0.73})_{37}RGO_{63}$ catalyst.

References:

1. W. Hummers and R. Offeman, *J Am Chem Soc*, 1958, 80, 1339.
2. H. J. Monkhorst and J. D. Pack, *Physical Review B*, 1976, 13, 5188.
3. G. Giovannetti, P. Khomyakov, G. Brocks, V. v. Karpan, J. Van den Brink and P. J. Kelly, *Physical review letters*, 2008, 101, 026803.
4. A. Gangula, R. Podila, L. Karanam, C. Janardhana and A. M. Rao, *Langmuir*, 2011, 27, 15268-15274.
5. P. Deka, R. C. Deka and P. Bharali, *New Journal of Chemistry*, 2014, 38, 1789-1793.
6. B. Baruah, G. J. Gabriel, M. J. Akbashev and M. E. Booher, *Langmuir*, 2013, 29, 4225-4234.
7. W. Zhang, Y. Sun and L. Zhang, *Industrial & Engineering Chemistry Research*, 2015, 54, 6480-6488.
8. Z. Zheng, Q. Huang, H. Guan and S. Liu, *RSC Advances*, 2015, 5, 69790-69799.
9. C. Kästner and A. F. Thünemann, *Langmuir*, 2016, 32, 7383-7391.
10. Y.-g. Wu, M. Wen, Q.-s. Wu and H. Fang, *The Journal of Physical Chemistry C*, 2014, 118, 6307-6313.
11. L. Zhang, T. Wu, X. Xu, F. Xia, H. Na, Y. Liu, H. Qiu, W. Wang and J. Gao, *Journal of Alloys and Compounds*, 2015, 628, 364-371.
12. Z. Jiang, J. Xie, D. Jiang, X. Wei and M. Chen, *CrystEngComm*, 2013, 15, 560-569.
13. A. Wang, H. Yin, H. Lu, J. Xue, M. Ren and T. Jiang, *Langmuir*, 2009, 25, 12736-12741.
14. Z. Zhu, X. Guo, S. Wu, R. Zhang, J. Wang and L. Li, *Industrial & Engineering Chemistry Research*, 2011, 50, 13848-13853.
15. J. Huang, S. Vongehr, S. Tang, H. Lu and X. Meng, *The Journal of Physical Chemistry C*, 2010, 114, 15005-15010.
16. M. M. Kumari, J. Jacob and D. Philip, *Spectrochimica Acta Part A: Molecular and Biomolecular Spectroscopy*, 2015, 137, 185-192.

17. H. Fu, X. Yang, X. Jiang and A. Yu, *Langmuir*, 2013, 29, 7134-7142.
18. R. Dhanda and M. Kidwai, *Journal of Materials Chemistry A*, 2015, 3, 19563-19574.
19. M. Kumar and S. Deka, *ACS applied materials & interfaces*, 2014, 6, 16071-16081.
20. S. Senapati, S. K. Srivastava, S. B. Singh and H. N. Mishra, *Journal of Materials Chemistry*, 2012, 22, 6899-6906.
21. Y. Tian, Y. Liu, F. Pang, F. Wang and X. Zhang, *Colloids and Surfaces A: Physicochemical and Engineering Aspects*, 2015, 464, 96-103.
22. Z. Ji, X. Shen, G. Zhu, H. Zhou and A. Yuan, *Journal of Materials Chemistry*, 2012, 22, 3471-3477.
23. M. Gopiraman, D. Deng, S. Saravanamoorthy, I.-M. Chung and I. S. Kim, *RSC Advances*, 2018, 8, 3014-3023.
24. S. Tang, S. Vongehr and X. Meng, *The Journal of Physical Chemistry C*, 2009, 114, 977-982.
25. N. Meng, S. Zhang, Y. Zhou, W. Nie and P. Chen, *RSC Advances*, 2015, 5, 70968-70971.
26. Z. Dong, X. Le, X. Li, W. Zhang, C. Dong and J. Ma, *Applied Catalysis B: Environmental*, 2014, 158, 129-135.
27. S. Gao, Z. Zhang, K. Liu and B. Dong, *Applied Catalysis B: Environmental*, 2016, 188, 245-252.
28. B. Ma, M. Wang, D. Tian, Y. Pei and L. Yuan, *RSC Advances*, 2015, 5, 41639-41645.
29. B. Vellaichamy and P. Periakaruppan, *RSC Advances*, 2016, 6, 88837-88845.
30. K. Hareesh, R. Joshi, D. Sunitha, V. Bhoraskar and S. Dhole, *Applied Surface Science*, 2016, 389, 1050-1055.
31. C. Sarkar and S. K. Dolui, *RSC Advances*, 2015, 5, 60763-60769.
32. S. Bai, X. Shen, G. Zhu, M. Li, H. Xi and K. Chen, *ACS applied materials & interfaces*, 2012, 4, 2378-2386.
33. J. Yang, X. Shen, G. Zhu, Z. Ji and H. Zhou, *RSC Advances*, 2014, 4, 386-394.
34. L. Rout, A. Kumar, R. S. Dhaka, G. N. Reddy, S. Giri and P. Dash, *Applied Catalysis A: General*, 2017, 538, 107-122.
35. X. Li, X. Wang, S. Song, D. Liu and H. Zhang, *Chemistry-A European Journal*, 2012, 18, 7601-7607.
36. J. Li, C.-y. Liu and Y. Liu, *Journal of Materials Chemistry*, 2012, 22, 8426-8430.
37. M. Zhu, C. Wang, D. Meng and G. Diao, *Journal of Materials Chemistry A*, 2013, 1, 2118-2125.
38. P. Song, J.-J. Feng, S.-X. Zhong, S.-S. Huang, J.-R. Chen and A.-J. Wang, *RSC Advances*, 2015, 5, 35551-35557.
39. B. Naik, S. Hazra, V. S. Prasad and N. N. Ghosh, *Catalysis Communications*, 2011, 12, 1104-1108.
40. B. K. Ghosh, S. Hazra, B. Naik and N. N. Ghosh, *Journal of nanoscience and nanotechnology*, 2015, 15, 6516-6523.
41. S. Wang, X. He, L. Song and Z. Wang, *Synlett*, 2009, 2009, 447-450.
42. X. Zhang and A. Corma, *Angewandte Chemie*, 2008, 120, 4430-4433.
43. G.-P. Yong, D. Tian, H.-W. Tong and S.-M. Liu, *Journal of Molecular Catalysis A: Chemical*, 2010, 323, 40-44.
44. A. Elhampour, M. Malmir, E. Kowsari and F. Nemati, *RSC Advances*, 2016, 6, 96623-96634.
45. Z. Li, Z. Jiang and W. Su, *Green Chemistry*, 2015, 17, 2330-2334.
46. D.-H. Zhang, G.-D. Li, J.-X. Li and J.-S. Chen, *Chemical Communications*, 2008, 3414-3416.
47. D.-H. Zhang, H.-B. Li, G.-D. Li and J.-S. Chen, *Dalton Transactions*, 2009, 10527-10533.
48. J. Liu, F. Wang, Z. Gu and X. Xu, *Catalysis Communications*, 2009, 10, 868-871.
49. H. Liu, J. Bai, S. Wang, C. Li, L. Guo, H. Liang, T. Xu, W. Sun and H. Li, *Colloids and Surfaces A: Physicochemical and Engineering Aspects*, 2014, 448, 154-159.
50. Q. Wang, C. Li, J. Bai, W. Sun and J. Wang, *Journal of Inorganic and Organometallic Polymers and Materials*, 2016, 26, 488-493.
51. Y. Tang, M. Yang, W. Dong, L. Tan, X. Zhang, P. Zhao, C. Peng and G. Wang, *Microporous and Mesoporous Materials*, 2015, 215, 199-205.

52. X. Wang, Z. Liang, F. Zhang, L. Yang and S. Xu, *Journal of materials science*, 2013, 48, 5899-5903.
53. X. Hu, J. Bai, C. Li, H. Liang and W. Sun, *European Journal of Inorganic Chemistry*, 2015, 2015, 3758-3763.
54. D. Yang, N. Yang and J. Ge, *CrystEngComm*, 2013, 15, 7230-7235.
55. G. Bian, P. Jiang, H. Zhao, K. Jiang, L. Hu, Y. Dong and W. Zhang, *ChemistrySelect*, 2016, 1, 1384-1392.
56. A. N. Prasad, B. Thirupathi, G. Raju, R. Srinivas and B. M. Reddy, *Catalysis Science & Technology*, 2012, 2, 1264-1268.
57. H. Sharghi, S. Ebrahimpourmoghaddam, M. M. Doroodmand and A. Purkhosrow, *Asian Journal of Organic Chemistry*, 2012, 1, 377-388.
58. H. Naeimi and V. Nejadshafiee, *New Journal of Chemistry*, 2014, 38, 5429-5435.
59. B. A. Kumar, K. H. V. Reddy, G. Satish, R. U. Kumar and Y. Nageswar, *RSC Advances*, 2014, 4, 60652-60657.
60. G. Kumaraswamy, K. Ankamma and A. Pitchaiah, *The Journal of organic chemistry*, 2007, 72, 9822-9825.
61. J. Yadav, B. S. Reddy, G. M. Reddy and D. N. Chary, *Tetrahedron Letters*, 2007, 48, 8773-8776.
62. H. Naeimi and Z. Ansarian, *Applied Organometallic Chemistry*, 2017.
63. B. K. Ghosh, S. Hazra and N. N. Ghosh, *Catalysis Communications*, 2016, 80, 44-48.
64. B. K. Ghosh, D. Moitra, M. Chandel, M. K. Patra, S. R. Vadera and N. N. Ghosh, *Catalysis Letters*, 2017, 147, 1061-1076.
65. D. Moitra, B. K. Ghosh, M. Chandel and N. N. Ghosh, *RSC Advances*, 2016, 6, 97941-97952.
66. Y. Zhou, T. He and Z. Wang, *Arkivoc*, 2008, 13, 80-90.
67. M. Varyani, P. K. Khatri and S. L. Jain, *Catalysis Communications*, 2016, 77, 113-117.